JOURNAL OF GLACIOLOGY

CAMBRIDGE UNIVERSITY PRESS

Evolution of the seasonal dynamics of the lake-terminating glacier Fjallsjökull, southeast Iceland, inferred using high-resolution repeat UAV imagery

Journal:	*Journal of Glaciology*
Manuscript ID	Draft
Manuscript Type:	Article
Date Submitted by the Author:	n/a
Complete List of Authors:	Baurley, Nathaniel; University of Southampton, Department of Geography and Environmental Science Hart, Jane; University of Southampton, Geography and Environment
Keywords:	Ice dynamics, Ice velocity, Glacier monitoring, Remote sensing, Glacier calving
Abstract:	Proglacial lakes are becoming ubiquitous at the termini of many glaciers worldwide, leading to increased glacier mass loss and terminus retreat, yet an understanding of the key processes forcing their behaviour is lacking. This study utilised high-resolution repeat uncrewed aerial vehicle (UAV)-Structure from Motion (SfM) imagery to provide insights into the changing dynamics of Fjallsjökull, a large lake-terminating glacier in southeast Iceland, across the 2019 and 2021 summer melt seasons. We show that the overall dynamics of the glacier are controlled by the ~120 m deep bedrock channel under the study region, which has caused the glacier to flow faster as it enters deeper water, leading to increased ice

	acceleration, thinning and retreat, with the glacier decoupled from local climate as a result. The close correspondence between ice velocity and surface thinning suggests the implementation of the dynamic thinning feedback mechanism, with such a response likely to continue in future until the glacier recedes out of the bedrock channel into shallower water. As a result, these findings clearly indicate the complex nature of the calving process, highlighting the need for continued monitoring of lake-terminating glaciers in order to better understand and predict how they may respond in future.

Evolution of the seasonal dynamics of the lake-terminating glacier Fjallsjökull, southeast Iceland, inferred using high-resolution repeat UAV imagery

Nathaniel R. Baurley[1]* and Jane K. Hart[1]

[1]Geography and Environmental Science, University of Southampton, Southampton, United Kingdom.

***Correspondence:**
Nathaniel R. Baurley
n.baurley@soton.ac.uk

Keywords: uncrewed aerial vehicles, lake-terminating glaciers, glacier velocity, surface elevation change, glacier dynamics, structure from motion photogrammetry, glacier monitoring.

ABSTRACT

Proglacial lakes are becoming ubiquitous at the termini of many glaciers worldwide, leading to increased glacier mass loss and terminus retreat, yet an understanding of the key processes forcing their behaviour is lacking. This study utilised high-resolution repeat uncrewed aerial vehicle (UAV)-Structure from Motion (SfM) imagery to provide insights into the changing dynamics of Fjallsjökull, a large lake-terminating glacier in southeast Iceland, across the 2019 and 2021 summer melt seasons. We show that the overall dynamics of the glacier are controlled by the ~120 m deep bedrock channel under the study region, which has caused the glacier to flow faster as it enters deeper water, leading to increased ice acceleration, thinning and retreat, with the glacier decoupled from local climate as a result. The close correspondence between ice velocity and surface thinning suggests the implementation of the dynamic thinning feedback mechanism, with such a response likely to continue in future until the glacier recedes out of the bedrock channel into shallower water. As a result, these findings clearly indicate the complex nature of the calving process, highlighting the need for continued monitoring of lake-terminating glaciers in order to better understand and predict how they may respond in future.

1. INTRODUCTION

Continued and more intensive global climate warming, particularly over the last two decades, is driving patterns of glacier recession and mass loss (Huss and Hock, 2018; Farinotti and others, 2019; Marzeion and others, 2020). Consequently, it is now widely established that all glaciers worldwide are undergoing extensive retreat and mass loss, with such patterns forecast to continue over the coming decades (Gardner and others, 2013; Huss and Hock, 2015; Zemp and others, 2019). This has important consequences for their meltwater contribution to global sea level rise (SLR) (Farinotti and others, 2019; Wouters and others, 2019; Hugonnet and others, 2021), as well as for regional hydrology due to the strong control glacier meltwater has on modulating down-glacier streamflow. This in turn affects freshwater availability, hydropower operations and sediment transport (Huss and Hock, 2018; Gärtner-Roer and others, 2019; Marzeion and others, 2020). Detailed glacier monitoring is, therefore, required, so that their future patterns of retreat and mass loss can be more accurately quantified (Paul and others, 2015; Gärtner-Roer and others, 2019; Hugonnet and others, 2021).

However, this relationship between climate and glacier retreat is distinctly more blurred for those glaciers that terminate in water, because in these settings retreat is instead often controlled by an additional and highly significant mass loss mechanism termed calving (Warren and Kirkbride, 2003; Chernos and others, 2016; Benn and Åström, 2018). Calving, otherwise known as frontal ablation, refers to the mass loss that can result from both the mechanical 'break off' of blocks of ice from the terminus, as well as from the direct melting of the terminus face through subaqueous melt (Truffer and Motyka, 2016; How and others, 2019; Carrivick and others, 2020). Although these processes are spatially and temporally complex, calving is important because it can decouple the dynamic behaviour of a glacier from climate, with factors other than variations in mass balance, such as changes in water depth and glacier geometry, exerting major controls on the flow velocity and retreat rate of these glaciers (Meier and Post, 1987; Howat and others, 2007; Carrivick and Tweed, 2013). Indeed, these factors can often cause calving glaciers to undergo significantly greater rates of retreat than would otherwise be observed if they lost mass by surface ablation alone (Warren and Kirkbride, 2003; Benn and others, 2007; Trüssel and others, 2013), and thus it is no surprise that in recent years many calving glaciers worldwide have undergone dramatic acceleration and retreat (e.g. Larsen and others, 2007; Howat and others, 2008; Sakakibara and Sugiyama, 2014; King and others, 2018). This potential for calving glaciers to exhibit a highly non-linear response to environmental forcing suggests they can contribute disproportionately to global SLR, further highlighting the importance of calving in regulating how such glaciers may respond in future (Benn and others, 2007; Carrivick and Tweed, 2013; Chernos and others, 2016).

The calving dynamics of marine-terminating glaciers have received the most attention in the literature over recent decades because the large and rapid losses often associated with these glaciers is particularly important for global SLR (Howat and others, 2007; Truffer and Motyka, 2016; Sakakibara and Sugiyama, 2018). However, much less is known about the changing dynamics of, and the future contributions to SLR from, lake-terminating glacier systems, despite the number of such systems increasing worldwide in response to continued glacier retreat, with such patterns of lake formation forecast to continue in future (Carrivick and others 2020; Shugar and others, 2020). Furthermore, while there has been an increase in the number of studies over recent years which have examined the changing dynamics of lake-terminating glaciers (e.g. Sakakibara and others, 2013; Chernos and others, 2016; King and others, 2018; Dell and others, 2019), the key processes forcing these changes are still not wholly understood, meaning further research is required so that the future dynamics and retreat patterns of these glaciers can be more accurately quantified (Carrivick and others, 2020; Shugar and others, 2020).

To date, much of our understanding of lake-terminating glacier dynamics stems from the application of satellite remote sensing, which facilitates the monitoring of these glaciers over a range of spatial (glacier-wide to regional) and temporal (days to decadal) scales with relatively low cost and effort (e.g. Sakakibara and Sugiyama, 2014; King and others, 2018; Baurley and others, 2020; Pronk and others, 2021). However, the relatively coarse spatial and temporal resolution of this data, and its susceptibility to certain weather conditions (e.g. cloud cover), can significantly affect the regularity and quality of the acquired data, particularly when monitoring changes over fine spatial and temporal scales (Lemos and others, 2018; Millan and others, 2019). Yet despite advances in recent years towards higher resolution satellites with shorter repeat intervals, it is still difficult to investigate those short-term (e.g. daily) variations in the dynamic behaviour of calving glaciers using satellite remote sensing alone (e.g. Sugiyama and others, 2015; Altena and Kääb, 2017; How and others, 2019).

The emergence of uncrewed aerial vehicles (UAVs) in cryospheric research over recent years may provide a sound alternative, offering rapid assessments of glacier surface dynamics at extremely high spatial (cm-scale) and temporal (sub-daily) resolutions (Whitehead and others, 2013; Ryan and others, 2015; Chudley and others, 2019). Indeed, when combined with modern, and relatively low-cost Structure from Motion (SfM) techniques, the UAV-SfM method allows for the generation of orthomosaics and DEMs of the ice surface and surrounding morphology at very high resolutions (e.g. Bash and others, 2018; Rossini and others, 2018; Yang and others, 2020). Furthermore, the ability to conduct rapid repeat surveys of the ice surface, due to the 'on demand' deployment of UAV systems, allows glaciologists the opportunity to undertake weekly, daily, or even sub-daily surveys of the ice surface, providing insights into glacial processes that would be nearly impossible to obtain using more traditional techniques (e.g. Immerzeel and others, 2014; Bash and others, 2018; Jouvet and others, 2019; Xue and others, 2021). Yet, despite enhancing our ability to monitor the rapidly changing glacial landscape and its future evolution (e.g. Ryan and others, 2015; Rossini and others, 2018), the method has not been extensively deployed for the investigation of lake-terminating glacier dynamics, with the work of Wigmore and Mark (2017), who investigated the dynamics of the slow-moving debris-covered tongue of Llaca Glacier, Peru, being the only study in the literature to date. Therefore, to better understand the dynamic behaviour of lake-terminating glaciers, there is a need to expand the deployment of such methods across a greater number of study glaciers in order to fully explore its potential.

In this study, we utilise repeat high-resolution UAV-SfM imagery to assess the changing dynamic behaviour of Fjallsjökull, a large and dynamic lake-terminating glacier in southeast Iceland, over the 2019 and 2021 summer melt season. Through repeat surveys of the calving front, we quantify short-term (daily to weekly) variations in both the ice velocity, as well as changes in ice surface elevation, and how these vary spatially across the study region. Subsequently, we demonstrate how these dynamic variations are predominately being forced by the presence of a deep bedrock channel under the study region, which has caused the glacier to speed up as it continually recedes into deeper water, leading to the implementation of a positive feedback mechanism. We suggest these findings may provide an indication as to how other, similar lake-terminating glaciers, both in Iceland and further afield, may respond in future, providing a methodological basis on which future research can be developed.

2. STUDY AREA

Fjallsjökull (64°01′N, 16°25′W) is a piedmont outlet lobe situated on the southern side of the Vatnajökull Ice Cap, in southeast Iceland (Fig. 1) (Evans and Twigg, 2002; Dell and others, 2019). In 2010 the glacier covered an area of ~44.6 km^2, had a volume of 7.0 km^3 and was ~12.9 km long (Hannesdóttir and others, 2015). Like many glaciers in Iceland, Fjallsjökull has undergone significant recession over the last century. Measurements at the land-terminating southern margin indicate that >1.7 km of retreat occurred between 1934-2019 (Hannesdóttir and others, 2015; WGMS, 2020), with a particularly heightened rate of retreat (~35 m a^{-1}) observed since the early 2000s (Dell and others, 2019; Chandler and others, 2020).

This ongoing retreat has revealed a substantial overdeepening, which attains a maximum depth of ~206 m, is ~3 km wide and ~4 km long (Fig. 1d) (Magnússon and others, 2012; Dell and others, 2019). The emergence of this overdeepening has led to the development of the large proglacial lake Fjallsárlón (~3.7 km^2 in 2018), the third largest in southeast Iceland, into which the glacier currently terminates (Guðmundsson and others, 2019; Chandler and others, 2020). Recent research by Dell and others (2019) has indicated that the subglacial topography and continued expansion of Fjallsárlón have become important controls for the overall dynamics of the glacier, particularly over recent decades, warranting further research into this rapidly changing and highly dynamic glacier (Guðmundsson and others, 2019; Chandler and others, 2020).

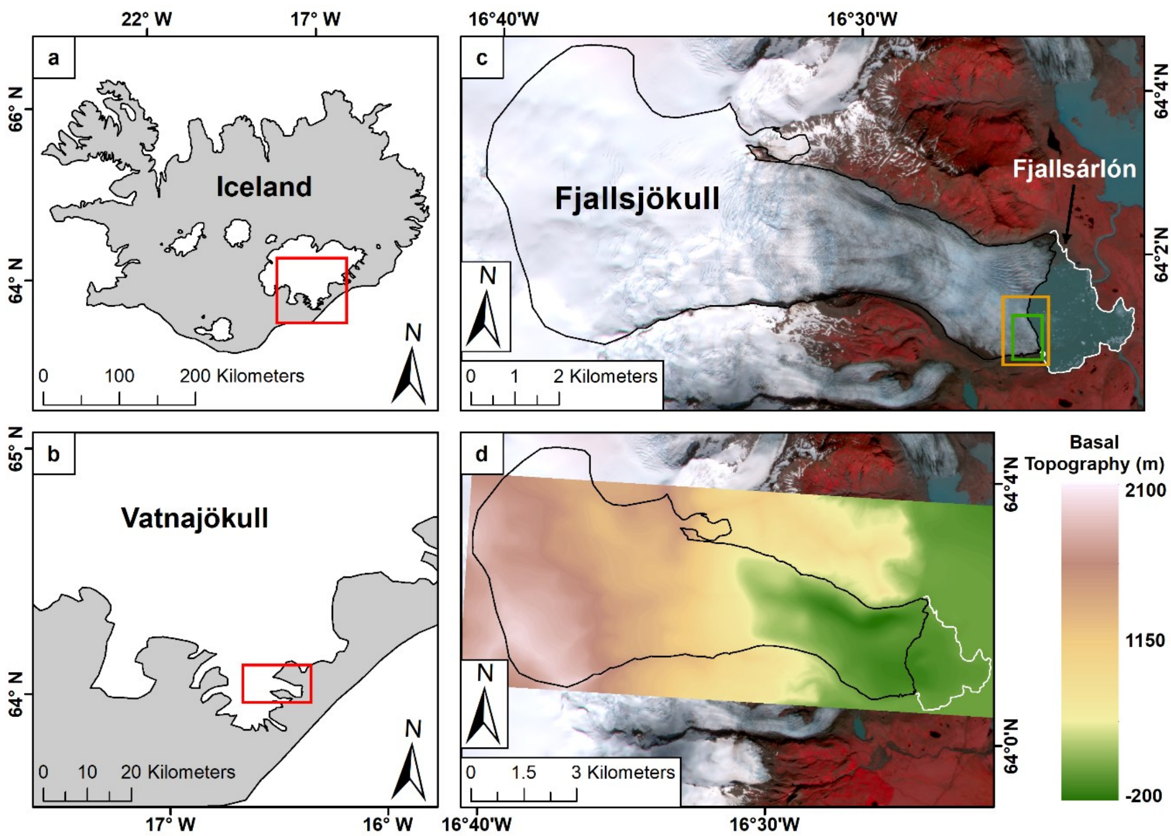

Fig. 1. Location map of Fjallsjökull. (a) Location of Fjallsjökull within Iceland, and (b) within the Vatnajökull Ice Cap. (c) Area of Fjallsjökull and Fjallsárlón as of July 2021. Glacier outline obtained from the GLIMS database, with the green and orange boxes delineating the areal coverage of the UAV-SfM surveys undertaken in 2019 and 2021, respectively. These also reflect the glacier extents shown in Figs. 2b, 3b and 6-9. (d) Bedrock topography of Fjallsjökull, interpolated from data provided to the author by E. Magnússon. Glacier outline and lake area as before. Background is a 4-band false-colour PlanetScope acquisition from 7 July 2021.

3. DATA AND METHODS

3.1 Repeat UAV-SfM Surveys

3.1.1 2019 Field Season

The UAV system utilised during the summer of 2019 was a 3DR Solo quadcopter equipped with a MAPIR Survey 3 camera, comprising a 12-megapixel Sony Exmor R IMX117 sensor and a HFOV 19 mm lens to allow the capture of 24-bit JPG photos at a resolution of 4000x3000 pixels (Fig. 2a). The camera was also equipped with an external u-blox NEO-M8 GPS/GNSS module that automatically recorded the time, date, and geographical position of each image with a positional accuracy of ~10 m. For all flights, the camera was set to automatically capture images every two seconds, which provided the best image quality based on UAV elevation and speed. In addition, camera settings for all flights were pre-set with the autofocus on, an ISO of 200, and with an automatic shutter speed due to the likelihood of differential surface and lighting conditions over the glacier (e.g. Immerzeel and others, 2014; Wigmore and Mark, 2017). All other settings were kept as standard.

UAV-SfM surveys were conducted over a ~0.5 km^2 region of the lower terminus of Fjallsjökull across one week in early July, and one week in mid-September 2019 during daylight hours. Each survey comprised a mosaic of several flights, however, due to inclement weather only three full surveys were completed (6 and 7 July 2019, 21 September 2019), with partial coverage of the study region obtained on the other survey days (Table 1).

Table 1. Details of each survey undertaken in July and September 2019.

Date	Time	Number of Flights	Number of Survey Lines	Total Area Covered (km^2)	Number of Photos
5 Jul 2019	14:11 – 15:23	4	8	0.289	568
6 Jul 2019	10:43 – 13:45	7	14	0.511	1006
7 Jul 2019	11:14 – 13:10	7	14	0.511	997
9 Jul 2019	10:06 – 10:59	4	8	0.289	550
19 Sep 2019	12:14 – 12:21	4	8	0.289	554
20 Sep 2019	14:33 – 15:07	3	6	0.219	404
21 Sep 2019	8:57 – 10:20	7	14	0.511	1012

All survey routes were designed using the free open-source software package 'Mission Planner' (http://ardupilot.org/planner/), with flight lines constructed approximately orthogonal to ice flow direction (Fig. 2b). All flights were flown autonomously at a constant elevation of ~100 m above ground level (AGL), resulting in a ground sampling distance (GSD) of ~0.03 m. To ensure optimal spatial coverage (e.g. Jouvet and others, 2019), all flights were flown at a constant speed of 5 m s^{-1}, resulting in an image overlap and sidelap of 92% and 70%, respectively. Each flight was also designed to ensure sufficient inclusion of stable ground areas adjacent to the glacier for use in the uncertainty assessment (Section 4.1).

Although the UAV camera was equipped with an external GPS, the positional accuracy of the module was too coarse for the needs of this study. To increase the accuracy of the final models a set of ground control points (GCPs) were deployed across the study site. The GCPs used here were high contrast, thick plastic markers, 1x1 m in size, with a clearly defined centroid to aid in locating the target centre during processing (Fig. 2c), with the centre position of each GCP recorded in the field using a Leica GS09 with an accuracy of <0.01 m. Seven GCPs were originally deployed around the study site at the start of fieldwork on 5 July 2019, although this was then increased to nine markers two days later. In comparison, eleven markers were deployed around the study site at the start of fieldwork on 19 September 2019 (Fig. 2d).

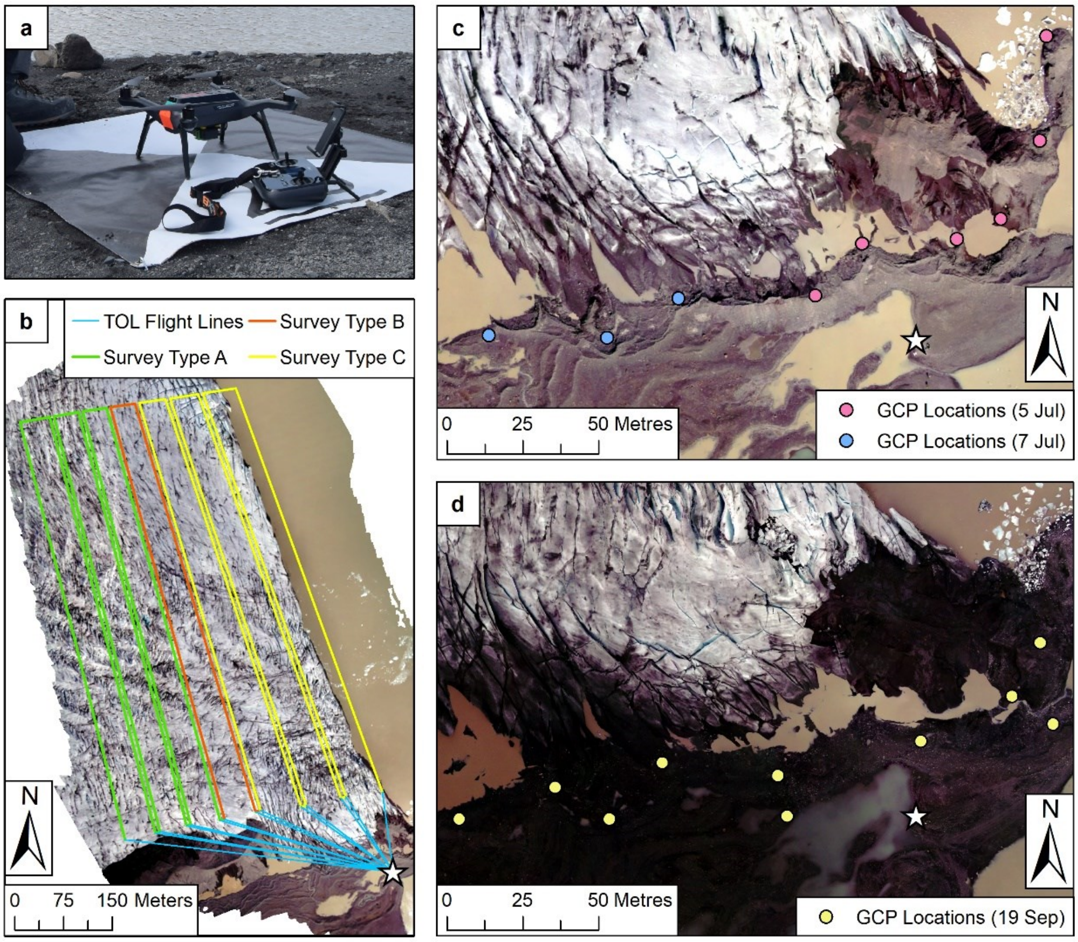

Fig. 2. (a) The 3DR Solo quadcopter used to undertake the UAV-SfM surveys in 2019. (b) Areal coverage of the different survey types flown over the study region in 2019: "Type A" (complete coverage), "Type B" (half coverage) and "Type C" (limited coverage). Take-off and landing (TOL) point is given by the white star. (c) GCP locations on 5 and 7 July. All GCPs were resurveyed, and three more added on 7 July due to the loss of the northernmost GCP between 6 and 7 July. (d) GCP locations on 19 September. White star in (c) & (d) as before. Background is the UAV-SfM orthomosaic from 7 July (b) & (c), and 19 September (d) 2019.

It is always preferable to place GCPs as evenly as possible across the area of interest to ensure a more robust and high-quality model output (James and Robson, 2012; Gindraux and others, 2017). However, this is not always possible when working in glacial environments due to the highly crevassed and hazardous nature of the ice surface, which may limit the ability to place GCPs evenly across the scene of interest (e.g. Immerzeel and others, 2014; Chudley and others, 2019). As a result, all GCPs were deployed across stable ground near the lateral margin of the glacier, ensuring good spread in the X, Y and Z planes.

3.1.2 2021 Field Season

For the July 2021 surveys, a DJI Inspire 2 equipped with a Zenmuse X4S camera was utilised, comprising a 20 megapixel 1" Exmor R CMOS sensor and a custom-engineered 8.8 mm/F2.8-11 compact lens, allowing for the capture of 24-bit JPEG photos at varying pixel resolutions (DJI 2021) (Fig 3a). For all flights, the camera was set to automatically capture images every three seconds to provide the best image quality. In addition, it was set to automatically adjust the image ISO with a user-defined shutter speed of 1/1000th to allow the capture of high-quality images over the glacier during variable lighting conditions (e.g. Jouvet and others, 2019; Chudley and others, 2021). Finally, differential carrier-phase GNSS (i.e. direct georeferencing) functionality was provided by an Emlid Reach M+ module, which was fixed to the underside of the UAV body and connected to the on-board camera, allowing the time and coordinates of each image to be logged with a post-positional accuracy of <0.05 m (Emlid, 2021a).

These surveys were conducted across two weeks in July 2021, between 11:30 and ~14:30, encompassing a ~0.9 km^2 region of the lower glacier terminus. Each survey once again comprised a mosaic of several flights, however, in contrast to the 2019 surveys full coverage of the study region was obtained on each survey day except 4 July 2021, where inclement weather meant only two flights were completed (Table 2).

Table 2. Details of each survey undertaken in July 2021.

Date	Time	Number of Flights	Number of Survey Lines	Total Area Covered (km^2)	Number of Photos
4 Jul 2021	13:10 – 13:45	2	8	0.572	490
6 Jul 2021	12:21 – 13:12	3	12	0.858	684
7 Jul 2021	13:35 – 14:32	3	12	0.858	684
8 Jul 2021	12:05 – 12:55	3	12	0.858	687
9 Jul 2021	12:01 – 12:51	3	12	0.858	684
10 Jul 2021	12:08 – 12:57	3	12	0.858	686
11 Jul 2021	12:43 – 13:49	3	12	0.858	684
12 Jul 2021	11:52 – 12:40	3	12	0.858	684
15 Jul 2021	11:59 – 12:50	3	12	0.858	684

The July 2021 surveys were designed using the commercially available app 'DJI Ground Station (GS) Pro' (https://www.dji.com/uk/ground-station-pro), with each survey route again constructed orthogonal to ice flow direction (Fig. 3b). All flights were flown autonomously at a constant elevation of 110 m AGL, resulting in a GSD of ~0.03 m. Meanwhile, to ensure optimal spatial coverage (e.g. Jouvet and others, 2019), the UAV was flown at a constant speed of 7.5 m s^{-1}, resulting in an image overlap and sidelap of 80% and 70%, respectively. As was the case for the 2019 surveys, each flight was also designed to ensure sufficient inclusion of stable ground areas adjacent to the glacier for use in the uncertainty assessment (Section 4.1).

To process the on-board differential carrier-phase GNSS data to a high degree of accuracy, a base station is required in order to provide differential corrections to the unit. For redundancy, two base stations were used in this study, a Leica GS1200 and an Emlid Reach RS2, with the former used for post-processing of the UAV-SfM data. Each base station was set up on an area of stable ground, ~200 m from the glacier with a clear sky view and with over 10 m between the two in order to avoid any potential interference. The height of the antenna above ground level was also recorded for each base station upon initial set-up each day to allow for Precise Point Positioning (PPP) post-processing using the AUSPOS online toolbox (https://gnss.ga.gov.au/auspos). To allow for optimum post-processing, both base stations were left to log for at least four hours while in the field, with at least one hour of logging before and after the first and last surveys were undertaken, respectively.

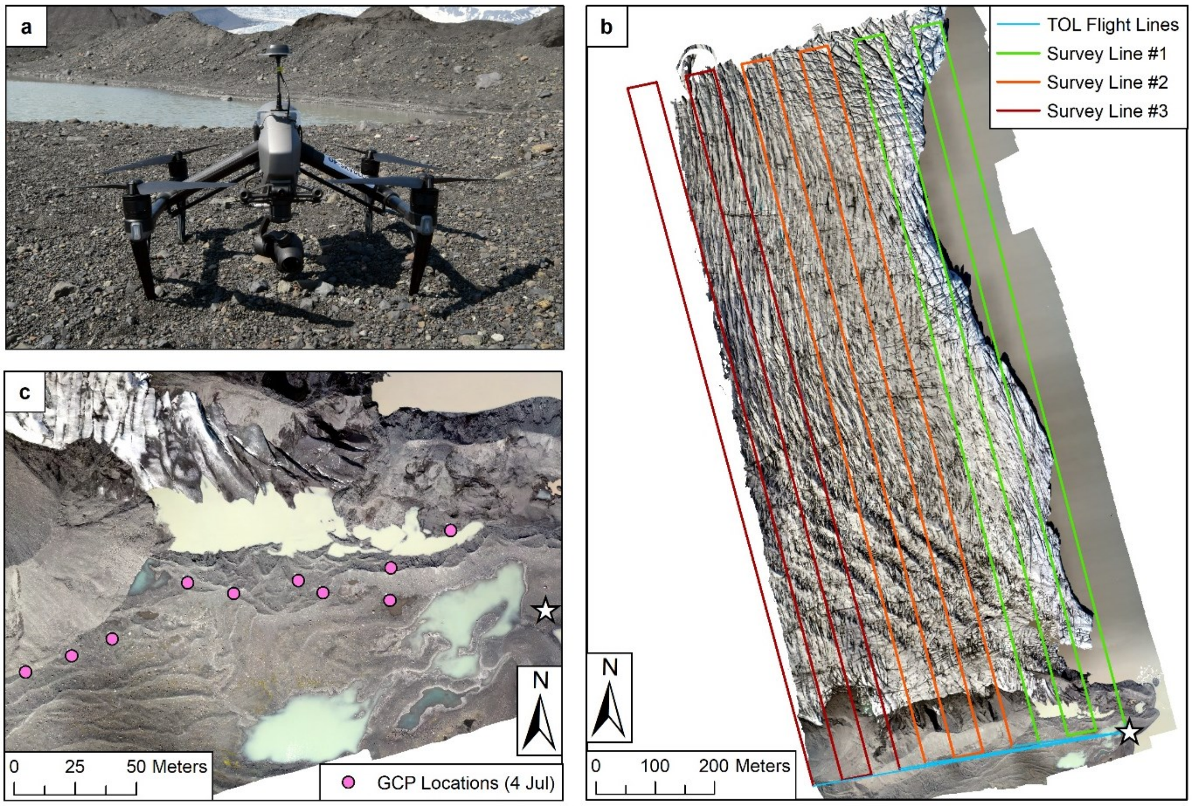

Fig. 3. (a) The DJI Inspire 2 used to undertake the UAV-SfM surveys in July 2021. (b) Areal coverage of the three surveys flown daily over the study region in July 2021, except for 4 July when only two surveys were completed (lines #1 and #2). Take-off and landing (TOL) point is given by the white star. (c) GCP locations on 4 July 2021, with the white star as in (b). Background in (b) & (c) is the UAV-SfM orthomosaic from 7 July 2021.

Although direct georeferencing functionality was provided by the Emlid Reach M+ module, a small network of ten GCPs were still deployed across the study site for redundancy (Fig. 3c). These GCPs were the same thick, high contrast 1x1 m markers used in 2019, and were again deployed across stable ground near the lateral margin of the glacier ensuring a good spread in the X, Y and Z planes, with the centre position of each GCP recorded using a Leica GS15 with an accuracy of <0.01 m. Although it was intended that all UAV-SfM imagery would be processed using the direct georeferencing method, a technical problem on 15 July meant no positional or timestamp data were recorded, and as such the images acquired from this day were georeferenced using the GCPs.

3.2 Post-Processing of UAV-SfM Data

The 2019 UAV-SfM imagery did not require any post-processing, so each image set (i.e. all the images acquired from one survey day) were directly loaded into Agisoft Metashape Professional v. 1.7 (Agisoft LLC, 2021) for 3D model generation. As a result, this section will focus solely on the post-processing undertaken on the imagery acquired in 2021.

3.2.1 GNSS Processing (Base and Rover)

The creation of highly accurate Post-Processed Kinematic (PPK) positional data strongly depends on the position of the user base station being precisely known (Tomsett and Leyland, 2021;

Baurley and others, 2022). As such, the raw positional base station data was first corrected using the AUSPOS online toolbox before being used to refine the positional data of the UAV. To accurately post-process this data, the positional information for each survey was first imported into RTKPOST_QT (https://docs.emlid.com/emlid-studio/). This was then used alongside the relevant post-processed base station file to update both the UAV track file and the positional information of each acquired image through forwards and backwards Kalman Filtering (e.g. Kim and Bang, 2019), providing camera locations accurate to <0.05 m (Emlid, 2022b).

3.2.2 Image-Position Matching

Next, the metadata of each image needed to be updated by using the position event files created in RTKPOST_QT. To do so, the images from each individual survey were imported into the software Toposetter (https://www.topodrone.org/news/event/software-toposetter-2-0/), before manually matching one image to an appropriate event file (i.e. so their metadata closely matched), with the software then matching subsequent images based on their nearest corresponding time. To allow maximum tolerance between image and position timestamp, and because the image timestamps are accurate to the nearest whole second, a tolerance of 1000 m s^{-1} was utilised to account for any possible rounding errors. Furthermore, as the images were captured approximately every three seconds along a flight line, by utilising this tolerance setting the likelihood that the event positions were assigned to an incorrect image was greatly reduced. Each post-processed image set was then imported into Agisoft Metashape, with each image assigned a positional accuracy of 0.05 m based on the output quality of the post-processing undertaken.

3.3 3D Model Generation (SfM Photogrammetry)

All image sets were processed into high resolution DEMs and orthomosaics of the ice surface and surrounding morphology using a SfM workflow (Westoby and others, 2012; James and Robson, 2012). Further detail on the SfM process can be found in Snavely and others (2008) and Fonstad and others (2013), with the specific workflow utilised in this study outlined below.

Firstly, an initial alignment procedure was undertaken based off the positional information of the imported imagery, resulting in a sparse point cloud made up of several hundred thousand points. All images were aligned using the highest accuracy setting and with no tie point limit to ensure more accurate estimations of camera positions, while maximising the number of pixel matches on low-contrast surfaces, like ice (Bash and others, 2018). For the 2019 surveys, the resultant sparse point clouds were created in an arbitrary coordinate system, so to align the models to real-world coordinates they first had to be georeferenced using the deployed GCPs. In this step, the centre of each GCP was manually marked within each photo and their coordinates (including accuracy and elevation) imported into Metashape to optimise spatial accuracy and 3D model geometry (Immerzeel and others, 2014; Rossini and others, 2018).

This step was not required for the 2021 data as the resultant point clouds were already directly georeferenced using the post-processed image positional data. The only exception to this was for those surveys undertaken on 15 July 2021, where a technical problem meant no positional information was recorded. Instead, the sparse point cloud was georeferenced using the GCP locations recorded in the field.

Following georeferencing, the camera positions were then optimised using the now-known reference coordinates to remove non-linear deformations and georeferencing errors from the final models (Agisoft LLC, 2021). The camera information from each georeferenced sparse point cloud could then be used to generate dense point clouds, made up of several hundred-million points. These dense point clouds were constructed using the high quality and aggressive depth filtering parameters, as is common in glacial research (e.g. Bash and others, 2018; Jouvet and others, 2019). The aggressive depth filtering parameter is particularly important as it removes noise from relatively smooth surfaces, such as snow or ice (Bash and others, 2018). Finally, DEMs and orthomosaics for each survey day were then produced, with these exported from Metashape at resolutions of 0.07 and 0.03 m (2019), and 0.05 and 0.03 m (2021), respectively, for further analysis.

3.4 Uncertainty Assessment

The relative uncertainty of the generated 3D models from both 2019 and 2021 were assessed by undertaking a repeat assessment of stable ground topography, following the method used by Tomsett and Leyland (2021) and Baurley and others (2022). This follows the principle that stable ground should be consistent between surveys and, therefore, any variations are indicative of the uncertainty in the system (e.g. Chudley and others, 2019; Yang and others, 2020). This in turn affects the level of confidence in the data and the level of change that can be detected. Indeed, because an extensive ground control network could not be deployed in either 2019 or 2021 due to the relative inaccessibility of the glacier surface, this stable ground assessment was essential to identify any errors between the generated 3D models.

For this assessment, an area of ice-free stable ground near the lateral margin of the glacier was selected that encompassed both shallow and steep topography and which was present in all the generated dense point clouds. This region was then extracted from each individual point cloud simultaneously to avoid any potential differences in stable ground extent. Once selected, each point cloud was differenced to each of the others in a pairwise fashion within CloudCompare v. 2.11.3, using the M3C2 algorithm developed by Lague and others (2013). This allowed the error to be assessed by comparing the median error, the Normalised Median Absolute Deviation (NMAD), as well as visualising their distribution, as outlined by Höhle and Höhle (2009). These errors could then be used to identify the minimum change detection threshold between surveys, which ensured that any differences present in the point clouds (and thus resultant DEMs and orthomosaics) represented actual change.

3.5 Glacier Surface Velocity

Feature tracking is a well-established technique for deriving glacier velocities from both satellite (e.g. Herman and others, 2011; Dehecq and others, 2015; Sakakibara and Sugiyama, 2018) and UAV (e.g. Ryan and others, 2015; Kraaijenbrink and others, 2016; Yang and others, 2020) imagery. Here, features were tracked using cross-correlation on orientation images (CCF-O), using the free software *CIAS* (https://www.mn.uio.no/geo/english/research/projects/icemass/cias/), which allows glacier surface displacements to be calculated with sub-pixel accuracy (Haug and others, 2010; Heid and Kääb, 2012). CCF-O was chosen in this study over other methods (such as NCC) because it uses the gradients between neighbouring pixel values to calculate displacements, rather than the raw digital values (Heid and Kääb, 2012; Robson and others, 2018). This reduces the impact of shadows and changing illumination conditions on the final displacements, both of which are common in glacierised regions (Heid and Kääb, 2012; Sakakibara and Sugiyama, 2018).

To quicken processing, each orthomosaic was resampled to a resolution of 0.25 m, before georeferencing each orthomosaic pair in ArcGIS before importing into CIAS. The processing parameters varied depending on the temporal separation between successive orthomosaics, with these given in Table 3. Resulting displacements were filtered by direction and magnitude (Robson and others, 2018). All displacements with a signal-to-noise ratio lower than 0.5 were removed, before manually identifying all displacements whose direction or magnitude varied by more than 20% to the mean values. The displacement fields were then interpolated using ordinary kriging to produce velocity rasters for each period.

Table 3. Processing parameters used in CIAS to produce velocity rasters of the ice surface, depending on the temporal separation between successive orthomosaics.

	Time Period Between Orthomosaics		
Parameter	**24 Hour (1 day)**	**48 Hour (2 day)**	**72 Hour (3 days)**
Reference Block (pixels)	15	15	15
Search Window (pixels)	20	30	40
Reference Grid (m)	1	1	1

To determine the uncertainty of the velocity calculations, displacements were measured over areas of stable ground that contained variable surface topography (e.g. Chudley and others, 2019; Jouvet and others, 2019). This analysis was undertaken over three distinct zones close to the glacier margin that were covered by both the 2019 and 2021 surveys, before calculating the combined stochastic standard deviation. Stable ground locations were chosen as theoretically no change should have occurred in these locations, and as such, they provide a good estimation for the accuracy of the feature tracking calculations.

3.6 Surface Elevation Change

To calculate the change in ice surface elevation, 2.5D DEM differentiation was utilised, whereby the earlier DEM was subtracted from the latter DEM to retrieve a spatially distributed map of vertical change. For the 2019 surveys, the two periods investigated were the 5-9 July and the 19-21 September. For the 2021 surveys, the period investigated was the 6-15 July because the DEM obtained on the 4 July covered a different (i.e. smaller) region compared to those DEMs from the subsequent eight days. To determine the uncertainty of the DEM differencing analysis, changes in elevation were measured over stable ground locations before calculating the combined stochastic standard deviation, following the same method used to assess the uncertainty of the velocity calculations (e.g. Chudley and others, 2019).

4. RESULTS

4.1 Uncertainty Assessment

The results of the stable ground assessment undertaken on the UAV-SfM point clouds importantly display similar levels of consistency between the different surveys from both 2019 and 2021. For the July 2019 comparisons (Fig. 4), the median error between points was between -0.045 and 0.069 m (1.5-2.3 GSD), with NMAD values no greater than ±0.227 and as low as ±0.097 m, indicating the difference between stable ground locations was relatively small. Interestingly, the lowest errors are found for 5-6, likely because the imagery acquired on these days were georeferenced using the same number of GCPs. Yet when comparing these dates to both the 7 and 9, the median error, and particularly the NMAD, have increased, indicating greater variation across stable ground. This may be because a greater number of GCPs, spread over a wider area, were used to georeference the models from 7 and 9, in comparison to 5 and 6 (Fig. 2c). This would have meant the stable ground locations on 5 and 6 were likely reconstructed differently to those on 7 and 9 (due to differing GCP numbers and distribution) (e.g. Gindraux and others, 2017), resulting in higher NMAD errors when comparing the two different sets of flight dates. This is supported by the fact that for 7-9 (which were georeferenced using the same GCPs), the median and NMAD have decreased to -0.051 m and ±0.102 m, respectively. In contrast, for the September 2019 data (Fig. 4), all errors show good similarity across the different comparisons, with median and NMAD errors of between 0.043 and 0.049 m (~1.5 GSD), and ±0.108 and ±0.146 m, respectively, across stable ground.

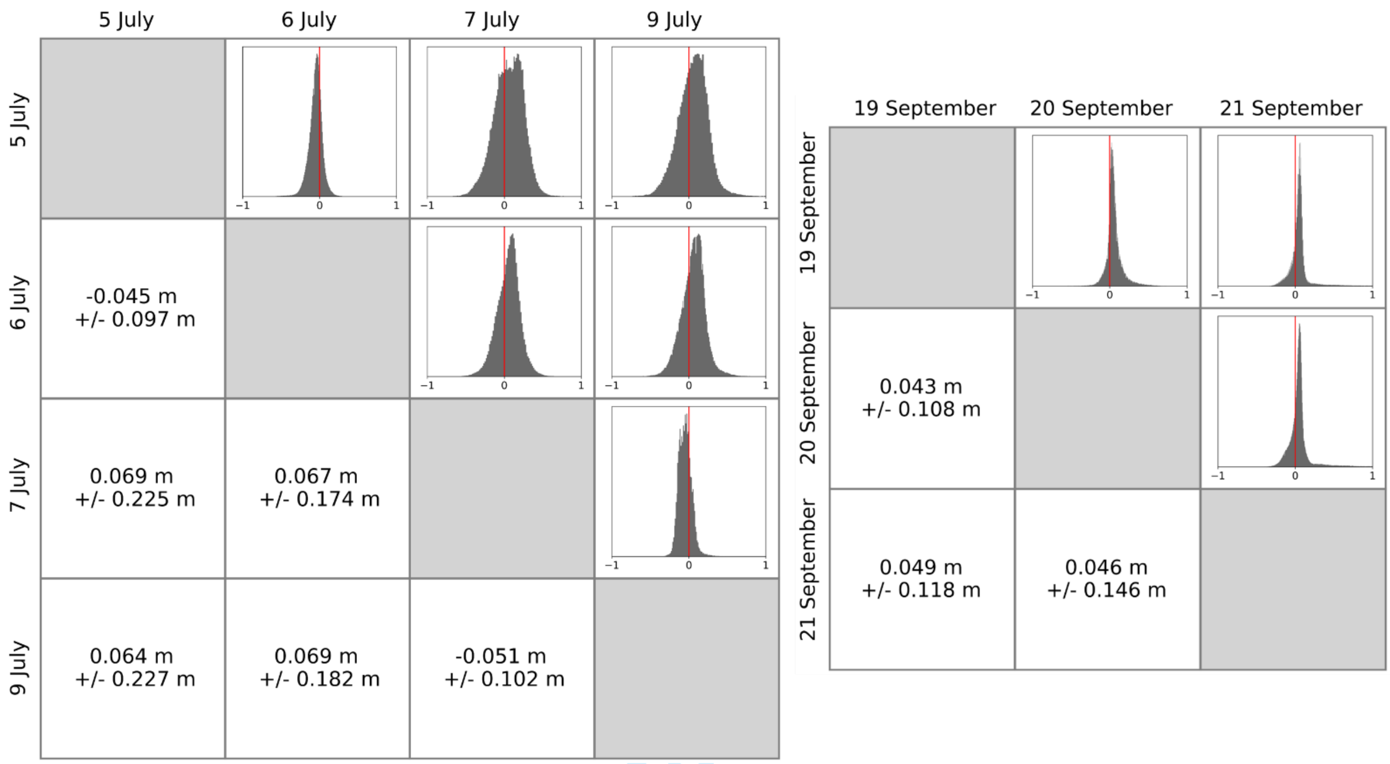

Fig. 4. Results of the uncertainty assessment for the UAV-SfM surveys undertaken in July (left) and September (right) 2019, calculated using M3C2 comparisons between each individual survey over areas of stable ground. Median and NMAD of errors are provided in the lower left of the matrix, whilst histograms showing the distribution of these errors are located in the upper right of the matrix.

For the July 2021 comparisons (Fig. 5), and in particular those comparisons across and between 6 and 15 July, both the median and NMAD errors again display good consistency between the different survey dates. Indeed, the median error was between 0.04 and -0.093 m (~1.3-3.5 GSD), with NMAD values of between ±0.04 and ±0.154 m, indicating that the differences were again small across stable ground. However, when comparing the error between 4 July and all other survey dates, the overall values are higher (particularly for the NMAD), with median and NMAD errors of up to 0.099 m (~3.3 GSD) and ±0.26 m obtained, respectively. The high NMAD values, alongside the visualisation of the histogram distributions, suggests a large spread in these data, which may be because only eight flight lines were flown on 4 July, whereas 12 were flown on all other dates (Table 2). As such, fewer images, captured from a smaller array of camera positions, would have been acquired over stable ground on this day, meaning a smaller number of images would have been made available for accurate scene reconstruction during SfM processing (Westoby and others, 2012), resulting in the high errors when comparing the stable ground locations from 4 July to all other survey dates. In contrast, it appears that the lack of direct georeferencing and subsequent reliance on GCPs for the 15 July has not impacted the model accuracy over stable ground regions, with similar distributions, and both median and NMAD values in the same order of magnitude as those surveys which utilised direct georeferencing.

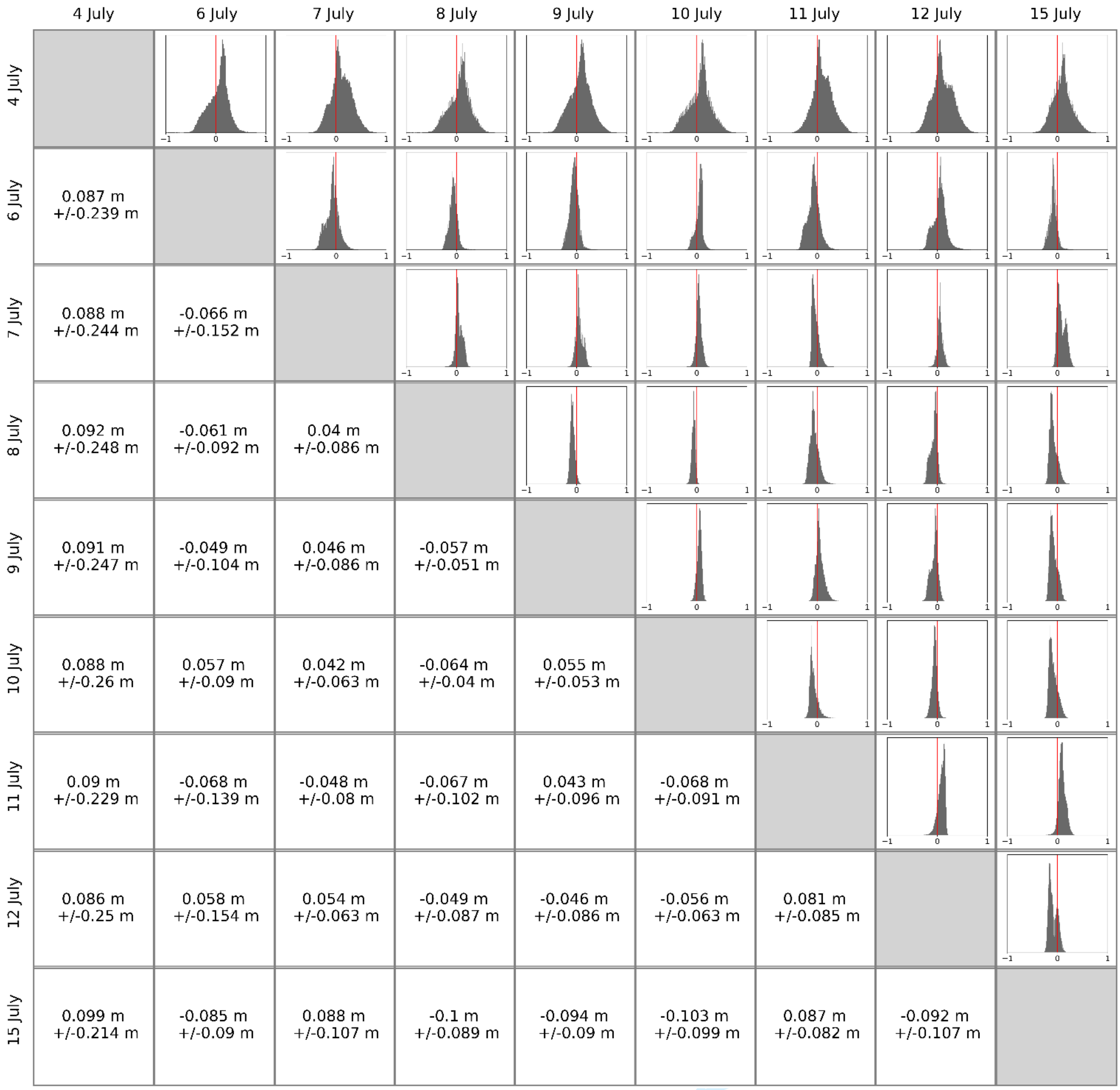

Fig. 5. Results of the uncertainty assessment for the July 2021 UAV-SfM surveys, calculated using M3C2 comparisons between each individual survey over the same areas of stable ground. As previously, the median, and NMAD of errors, as well as the histogram distribution of these errors, are shown.

Importantly, however, the errors from both July and September 2019, and July 2021, show very good agreement with those previous studies within glaciology that have undertaken their own UAV-SfM surveys at similar flying heights to those undertaken here. Across these studies, the range of reported errors was between 1.5 and ~3 times the GSD, with the flying heights of each respective survey ranging between 90 m and 110 m (e.g. Ely and others, 2017; Wigmore and Mark, 2017; Bash and others, 2018; Rossini and others, 2018; Xue and others, 2021). Overall, the results of the uncertainty assessment indicate that the errors found for all surveys across both years are smaller than the change expected over each period of interest (decimetre-metre scale), and are thus well within the realm of acceptability. This means that the orthomosaics and DEMs generated from these surveys can be reliably used to undertake further analysis of several different glaciological processes.

4.2 Glacier Surface Velocity

4.2.1 2019 Field Season

Overall, a clear pattern of surface velocity can be observed across the study region, where for all time periods in both July and September 2019 velocities clearly increase with increasing distance from the southern-grounded margin (Fig. 6). Between 5-6 July, velocities increase from ~0.35 ±0.09 m d^{-1} near the grounded margin up to ~0.80 ±0.09 m d^{-1} in the upper portion of the study region. Velocities near the calving front in this region peak at ~0.95 ±0.09 m d^{-1}, meaning this region of the glacier is flowing almost three times faster than those toward the grounded margin. Velocities over the rest of the study region range between ~0.40 and 0.75 ±0.09 m d^{-1}, resulting in an average velocity of ~0.47 ±0.09 m d^{-1}. Importantly, this overall pattern of velocity distribution, and indeed velocity magnitude, remains consistent across the subsequent days, with average velocities of 0.49 ±0.11 m d^{-1} and 0.51 ±0.10 m d^{-1} observed for 6-7, and 7-9 July, respectively, with peak values of ~0.95 m d^{-1} again reported in the upper portion of the study region for both time periods.

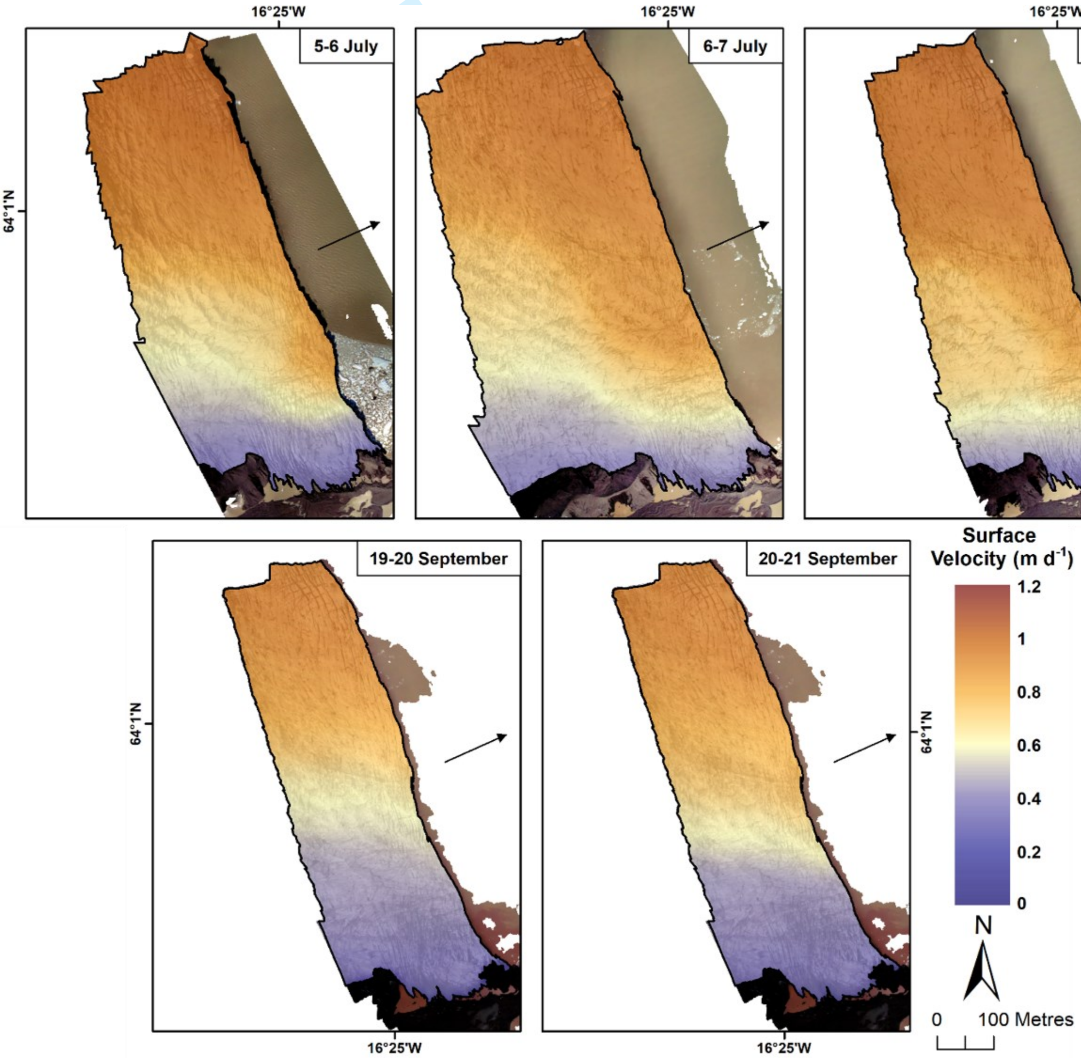

Fig. 6. Horizontal velocity fields for select time periods in July and September 2019, calculated using feature tracking on UAV-derived orthomosaics. Off-ice, stable-ground areas are shown for reference. Black arrows indicate ice flow direction. Background in each panel is the orthomosaic for the latter period, except in the first and last panels, when it is the former.

Although the results from September 2019 display the same overall pattern as observed in July 2019, the overall velocities are comparatively lower. Between 19-20 September, velocities increase from ~0.20 ±0.11 m d^{-1} at the margin to ~0.90 ±0.11 m d^{-1} near the calving front in the upper portion of the study region. Velocities over the rest of the study region range between 0.30 and 0.60 ±0.11 m d^{-1}, resulting in an average velocity for this period of ~0.32 ±0.11 m d^{-1}. Over the following 24-hour period (20-21 September), this overall pattern again remains consistent, with a slight increase in the average velocity observed (to 0.39 ±0.12 m d^{-1}), but with little change elsewhere, similar to what was observed in July. Interestingly, for all time periods in both July and September 2019, smaller-scale, more localised velocity variations can also be observed within this overall pattern, however, these are beyond the scope of the current study and will be discussed in detail in a future paper.

4.2.2 2021 Field Season

As was the case for both July and September 2019, the results from July 2021 display a similar overall pattern, with the velocity increasing with increasing distance from the southern-grounded margin. However, the key contrast between the two sets of results is that this region of Fjallsjökull was flowing faster overall in July 2021 than it was during either period in 2019 (Fig. 7). Between 6-7 July (the first day where full coverage of the study region was obtained), velocities increase from ~0.43 ±0.11 m d^{-1} near the grounded southern margin up to ~1.02 ±0.11 m d^{-1} in the upper portion of the study region. The highest velocities are once again found near the calving front in this region, with values peaking at ~1.20 ±0.11 m d^{-1}, which is around three times higher than those velocities observed near the margin. Over the rest of the study region, velocities range from between ~0.62 and 0.95 ±0.11 m d^{-1}, resulting in an average velocity of ~0.65 ±0.11 m d^{-1}, which is almost 0.2 m d^{-1} (~20%) faster than the average observed in July 2019.

Furthermore, this overall pattern of velocity distribution, and indeed velocity magnitude, is again consistent for all time periods in July 2021, with peak values of ~1.20 m d^{-1} reported in the upper portion of the study region for all time periods, in a similar fashion to what was observed in 2019. However, in contrast to 2019, there is greater variability in the average velocity calculated for each period in 2021, with values of 0.62 ±0.14, 0.82 ±0.10, 0.74 ±0.09, 0.69 ±0.11, 0.63 ±0.10, 0.62 ±0.09, and 0.65 ±0.12 m d^{-1} obtained for 4-6, 7-8, 8-9, 9-10, 10-11, 11-12, and 12-15 July, respectively. Such variability is likely a result of those smaller-scale and more localised velocity variations which occur within the overall velocity pattern, but over much shorter (e.g. daily) timescales. Although clearly of interest, as mentioned previously these localised variations are beyond the scope of the current study, and instead will be investigated in detail in a future paper.

4.3 Surface Elevation Change

4.3.1 2019 Field Season

Changes in ice surface elevation can be seen to have occurred between both 5-9 July, and 19-21 September 2019 (Fig. 7), and although the overall pattern of change is similar for both time periods, the magnitude of change does vary slightly. In the lower portion of the study region, near the southern grounded margin and away from the calving front, the surface elevation changes very little, with +1.00/-1.00 ±0.18 m and +0.50/-0.50 ±0.14 m of change observed in July and September 2019 respectively. Yet in the densely crevassed zone found in this region, and in the crevassed region north of this, more pronounced changes in elevation are found with proximity to the calving front, with between ~1.00 and 2.00 ±0.18 m of both positive and negative surface change observed between 5-9 July. In comparison, the changes in this region are much less pronounced between 19-21 September. Finally, and in a similar manner to the velocity results, these changes in surface elevation become more negative with increasing distance from the grounded southern margin. Indeed, the most negative changes have occurred in the upper portion of the study region, with between 2.00 and 2.50 ±0.18 m, and between 1.50 and 2.00 ±0.14 m of negative surface change observed here in July and September 2019 respectively.

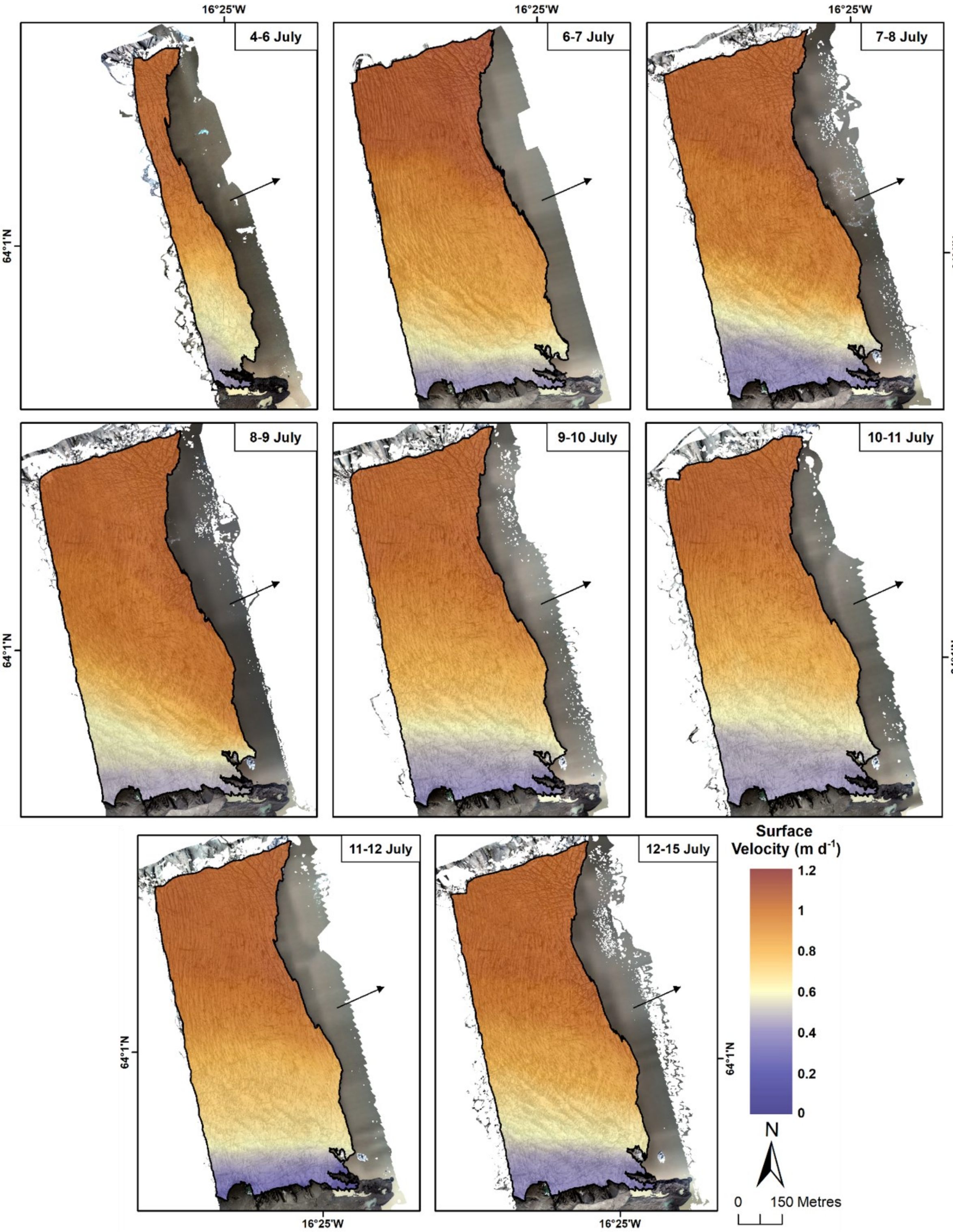

Fig. 7. Horizontal velocity fields for all time periods in July 2021, calculated using feature tracking on UAV-derived orthomosaics. Off-ice, stable-ground areas are shown for reference. Black arrows indicate ice flow direction. Background in each panel is the orthomosaic for the latter period, except in the first panel when it is the former.

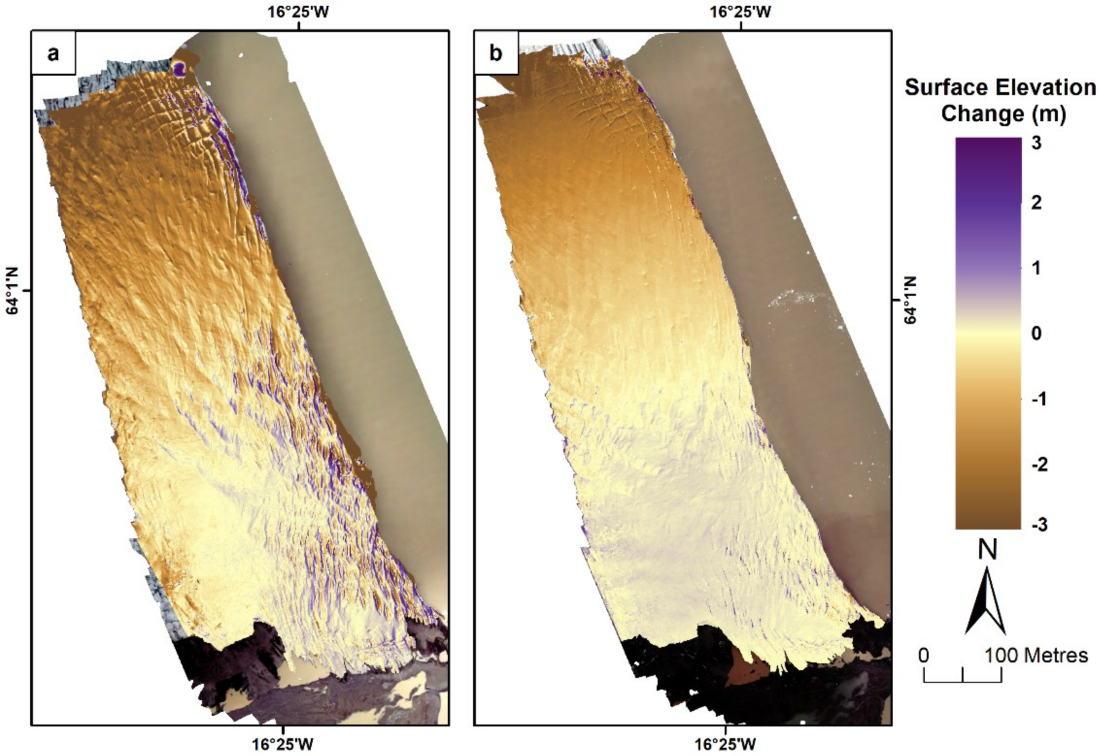

Fig. 8. Change in ice surface elevation between 5-9 July, and 19-21 September 2019, calculated using DEM differencing. Note the deep brown areas along the terminus, which represent the largest calving events that occurred over both respective periods. Background is the orthomosaic from 9 July and 19 September 2019, respectively.

4.3.2 2021 Field Season

Spatially variable changes in ice surface elevation have also occurred between 6-15 July 2021, however, the overall pattern and magnitude of this change strongly contrasts to the change observed during both time periods in 2019 (Fig. 8). In the lower portion of the study region, near to the grounded margin and away from the calving front, the change in surface elevation is slightly negative, with between -0.50 and ~-1.50 ±0.15 m of change observed. Within 200 m of the southern-grounded margin, however, these surface changes rapidly become more negative, with between 2.00 and 4.50 ±0.15 m of negative change observed.

Furthermore, the changes in surface elevation also generally become more negative with increasing distance from the southern-grounded margin, which agrees closely with the surface velocity results. Indeed, the most negative changes have occurred in the upper portion of the study region, near to the calving front, where upwards of ~5.50 ±0.15 m of negative change is observed. However, in those regions of densely crevassed ice (both near to, and away from, the calving front), this change is far more variable, with between ~3.50 and ~5.50 ±0.15 m of both positive and negative surface change observed in this time. Such a complex pattern is likely a result of the movement of these crevasses (and connected ridges) down-glacier between the two time periods of interest (Wigmore and Mark, 2017).

It is worth noting that in the DEMs from both 2019 and 2021, the deep brown areas found along the calving front likely represent large calving events (i.e. mass loss). In contrast, the deep brown and purple areas found to the far north and north-west of the study region (particularly in 2021) likely represent noise in the original DEMs, rather than actual change, due to the warping that can occur around the edges of a scene reconstructed from SfM when the GCPs, or the captured images, do not completely cover the area of interest (James and Robson, 2012; Gindraux and others, 2017).

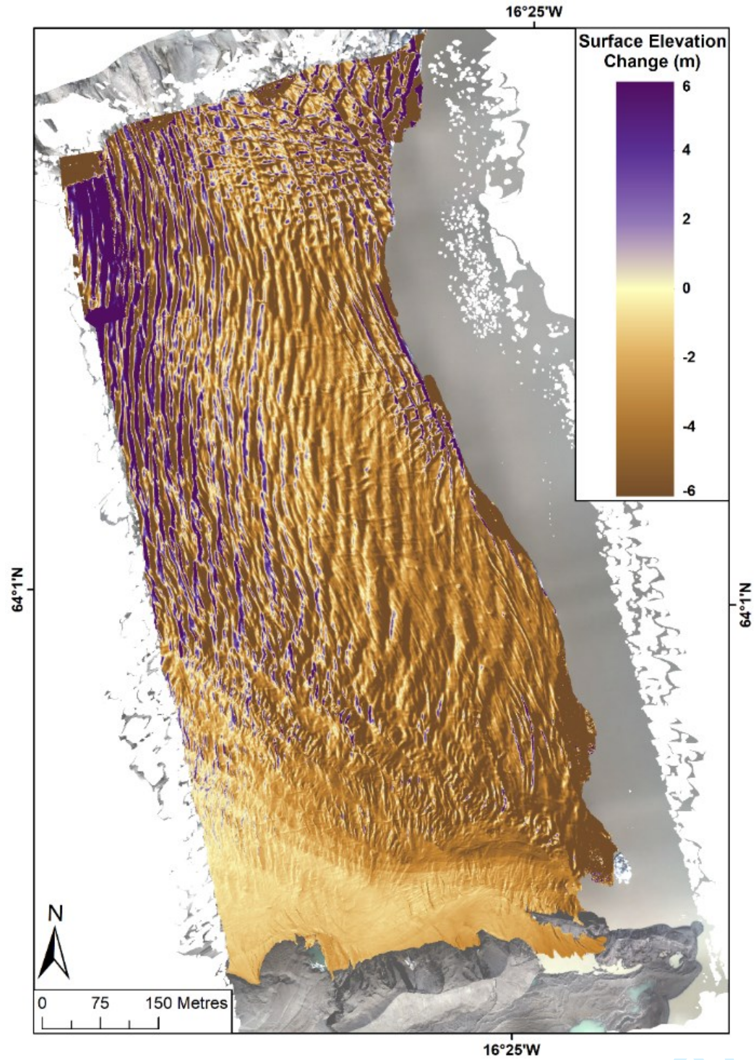

Fig. 9. Change in ice surface elevation for 6-15 July 2021, calculated using DEM differencing. Note the deep brown areas along the terminus, which represent the largest calving events that occurred over this period. Background is the orthomosaic from 15 July 2021.

5. DISCUSSION

5.1 Large-scale Velocity Variations and Links to Basal Topography

The overall velocity pattern (Figs. 6, 7) clearly indicates that velocities increase with increasing distance from the southern grounded margin, with the fastest velocities situated in the upper portion of the study region, near to the calving front. Importantly, however, such high velocities, and indeed the overall spatial variability in velocity that is observed in both 2019 and 2021, is strongly controlled by the particular basal topography underlying the study region (Fig. 1) (Magnússon and others, 2012; Dell and others, 2019). Information about the bedrock topography of Fjallsjökull is provided by Magnússon and others (2012), who acquired point measurements from across the ablation area (as well as its proglacial lake) through Radio-Echo Sounding surveys conducted between 1998 and 2006. Importantly, these data reveal that Fjallsjökull, and its proglacial lake Fjallsárlón, sit within a ~3 x 4 km subglacial trough, formed during the LIA advance, and which lies up to 206 m below sea level. Within this trough, two deeply incised bedrock channels can also be observed, one under the northern, and the other under the southern portion of the present-day terminus.

The southern bedrock channel, which is ~2 km by ~2 km and runs from ~0 m a.s.l. at the grounded southern margin to ~-120 m deep at its maximum, is of particular interest here as it directly corresponds to the area covered by the UAV-SfM surveys in both 2019 and 2021 (Fig. 10). Indeed, the region of elevated velocities consistently observed in the upper portion of the study region (~0.95 m d^{-1} in 2019 and ~1.2 m d^{-1} in 2021), directly corresponds to the deepest parts of the subglacial channel (~100-120 m below sea level). This is because glaciers flow faster when entering deeper water due to the inverse relationship that exists between the effective pressure (the difference between ice overburden and water pressure at the glacier bed) and basal drag (Warren and Kirkbride, 2003; Benn and others, 2007; Liu and others, 2020). Deeper water means greater up-ice propagation of lake water, which results in the glacier effectively being supported by the proglacial waterbody in the near-terminus region (Meier and Post, 1987; Carrivick and Tweed, 2013; Tsutaki and others, 2013). This, in turn, results in higher basal water pressures (equal to ice overburden), meaning the effective pressure is at, or close to zero, leading to increased bed separation, reduced basal drag and thus higher overall velocities (Benn and others, 2007; Sugiyama and others, 2011; Pronk and others, 2021).

This relationship between water depth and ice velocity likely explains (i) why elevated velocities are consistently found in the upper portion of the study region for all time periods in both years; (ii) why these velocities tend to increase towards the calving front (e.g. Sugiyama and others, 2015; Sakakibara and Sugiyama, 2018), and (iii) why velocities generally decrease as water depth decreases with increasing proximity to the grounded margin, indicating that the basal topography is likely exerting a first order control on the velocity of Fjallsjökull (Storrar and others, 2017; Dell and others, 2019).

Such high velocities in the upper portion of the study region also likely explain why up to ~2.50 ±0.18 m, and ~5.50 ±0.15 m of negative surface elevation change were observed in this region in 2019 and 2021, respectively (Figs. 8, 9). Elevated glacier velocities, driven by the deep bedrock channel, cause the ice surface to undergo longitudinal extension and thus thinning due to compressive vertical strain (Tsutaki and others, 2013; Shapero and others, 2016; Sakakibara and Sugiyama, 2018). This thinning reduces the thickness of the glacier, causing a reduction in the overburden pressure, which is already highly sensitive to any change in water depth, or indeed ice thickness (Benn and others, 2007; Sugiyama and others, 2011; Tsutaki and others, 2013).

This leads to a further reduction in the effective pressure, causing an additional increase in velocity and thus further longitudinal extension, thinning and the implementation of a positive feedback mechanism termed dynamic thinning (e.g. Howat and others 2007; Trüssel and others, 2013; Tsutaki and others, 2019; Pronk and others, 2021). Furthermore, the influence of the basal topography is highest where the glacier is thinnest (i.e. where the ratio between water depth and ice thickness is highest) (Benn and others, 2007; Storrar and others, 2017), which may also explain why the most negative changes in elevation are found where the channel is at its deepest.

Evidence for the occurrence of longitudinal extension is provided by the presence of large areas of transverse crevasses, particularly in the upper portion of the study region, as well as near the calving front. Such crevasses can only form where the rates of longitudinal extension are particularly high, and thus must be related to areas of fast ice flow (Tsutaki and others, 2013; Sakakibara and Sugiyama, 2018; Chudley and others, 2021). Furthermore, because the depth to which a crevasse can penetrate also increases with the amount of longitudinal extension, this mechanism can lead to an increase in calving at the terminus by increasing the likelihood of crevasses penetrating to the waterline and thus inducing failure (Benn and others, 2007; Shapero and others, 2016; King and others, 2018).

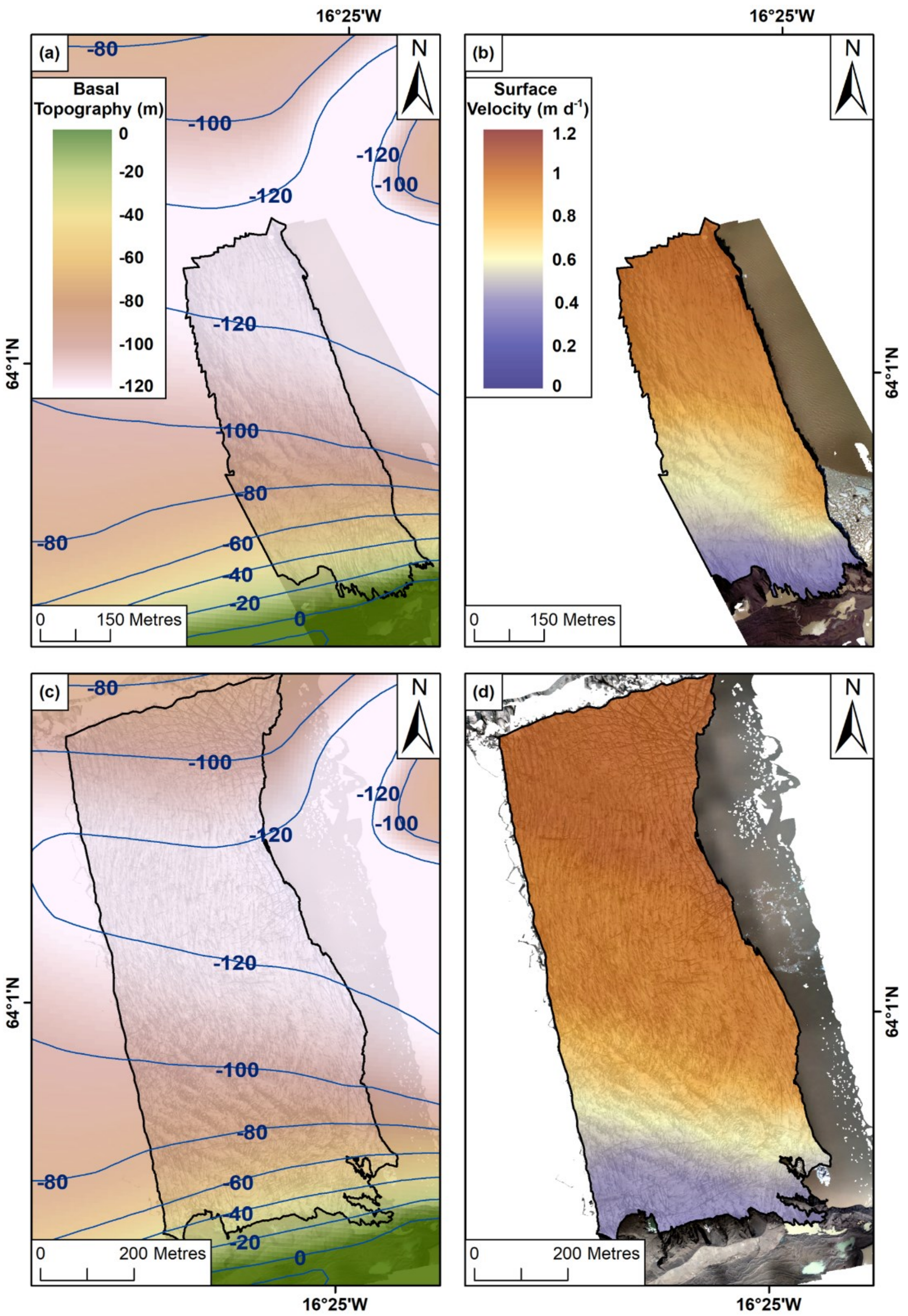

Fig. 10. Bedrock topography and surface velocity for select periods in July 2019 and 2021. (a) Bedrock topography under the southern portion of Fjallsjökull, interpolated from data provided to the author by E. Magnússon, indicating the presence of the 120 m deep subglacial channel under the study region. Blue lines represent basal contours at 20 m intervals. (b) Surface velocity for 5-6 July 2019, highlighting how the areas of fastest velocity are generally found where the bedrock topography is at its deepest. Background in both panels is the orthomosaic from 5 July 2019. (c) & (d) Same as (a) & (b), respectively, but for 7-8 July 2021. Background in both panels is the orthomosaic from 8 July 2021.

This mechanism can also induce calving by increasing the effect of buoyant forces acting on the normally grounded terminus (Trüssel and others, 2013; Dell and others, 2019). Any thinning of the ice, either by surface melting, retreat of the glacier into deeper water, or longitudinal extension, subjects the ice to buoyant (upward) forces (Boyce and others, 2007; Liu and others, 2020). To remain grounded the surface and basal gradients of a locally buoyant ice front must maintain a constant ratio, however, if this is not possible then the buoyant part of the terminus must rotate upwards to restore equilibrium, producing large bending forces near the junction with grounded terminal ice (Boyce and others, 2007; Benn and Åström, 2018). This then leads to rapid fracture propagation and calving, with pre-existing crevasses controlling the precise location of failure (Benn and others, 2007).

Any increase in calving via either of these two mechanisms can lead to an amplification of the dynamic thinning mechanism, which can exacerbate the retreat of calving glaciers in response to an initial forcing (Howat and others, 2008; Trüssel and others, 2013; Tsutaki and others, 2019). This is because calving leads to sudden mass loss at the terminus, and so to replace these losses the glacier must drawdown ice from higher elevations (Howat and others, 2008; Storrar and others, 2017). This increases the surface slope (and consequently the driving stress), leading to increased velocities (and, therefore, increased longitudinal extension), thinning, calving and further retreat (Benn and others, 2007; Shapero and others, 2016; Dell and others, 2019). Although a portion of the thinning observed across both time periods in 2019, as well as July 2021, would have likely occurred in response to surface ablation (e.g. Purdie and others, 2008; Trüssel and others, 2013), the magnitude of negative change observed suggests that it has primarily been forced by ice dynamics. For example, while the results from 2019 only cover five and three days, respectively, the fact that ~1.5-2 m of surface thinning is observed over both time periods, and that in both cases this area of lowering coincides with the area of heightened velocities, suggests that this feedback mechanism could be occurring in this region of Fjallsjökull. This is supported by the fact that away from this region of high velocities only small changes in surface elevation are observed (±0.5 m), which indicates that surface melt is the likely driver of surface change in these regions, rather than ice dynamics.

This suggestion is further strengthened by the field data from July 2021, which not only covered a longer time period (~10 days), but also a larger area than was possible in 2019. Indeed, up to ~5.50 m of surface thinning was observed in the upper portion of the study region during this period, with this again corresponding to the area of highest velocities. However, and perhaps more importantly, this overall pattern of surface thinning was not limited solely to the upper region. Rather, this region had increased in size, meaning a much larger portion of the overall study region was now characterised by these strongly negative surface changes. For example, in the lower portion of the study region, between 3.5 and 4.5 m of negative change were observed in this period, yet two years' prior, this same region was characterised by only ~1-1.5 m of negative change. It is important to again reiterate that although a portion of this thinning would have likely occurred in response to surface ablation, the magnitude of negative change observed suggests that it has primarily been forced by ice dynamics. This not only confirms that dynamic thinning is occurring at Fjallsjökull, but also suggests that it may now be impacting upon a much larger region of the glacier than it was in 2019. Several previous studies of lake-terminating glacier dynamics have also observed an increase in the areal extent of the dynamic thinning mechanism over time (e.g. Trüssel and others, 2013; King and others, 2018; Liu and others, 2020), reiterating its importance as a key forcing mechanism for the dynamics of Fjallsjökull.

It is important to note that other processes are likely also influencing the dynamics of Fjallsjökull (e.g. thermal notch-induced calving), with these being responsible for the localised velocity variations described in Section 4.2. However, these processes, and their influence on the dynamics of the glacier, are beyond the scope of the current study and will instead be discussed in detail in a future paper. This is due to the different spatial and temporal scales over which they operate compared to the bedrock topography-driven dynamic response discussed detail here.

Therefore, the overall spatial variations in velocity that were observed in both 2019 and 2021 are strongly linked to the location and depth of the bedrock channel, with a summary of the processes occurring in this region of Fjallsjökull given in Fig. 11. Velocities are greatest where the channel is deepest because glaciers flow faster when entering deeper water due to the inverse relationship that exists between the effective pressure and basal drag (Warren and Kirkbride, 2003; Carrivick and Tweed, 2013). This has caused the ice surface to undergo longitudinal extension (thinning), increasing the likelihood of crevasses penetrating to the waterline and inducing calving failure (Benn and others, 2007). This has resulted in increased mass loss and retreat, causing a further increase in ice velocity, and consequently, longitudinal extension, leading to the implementation of the dynamic thinning feedback mechanism in this region of Fjallsjökull (e.g. Trüssel and others, 2013; Tsutaki and others, 2013, 2019).

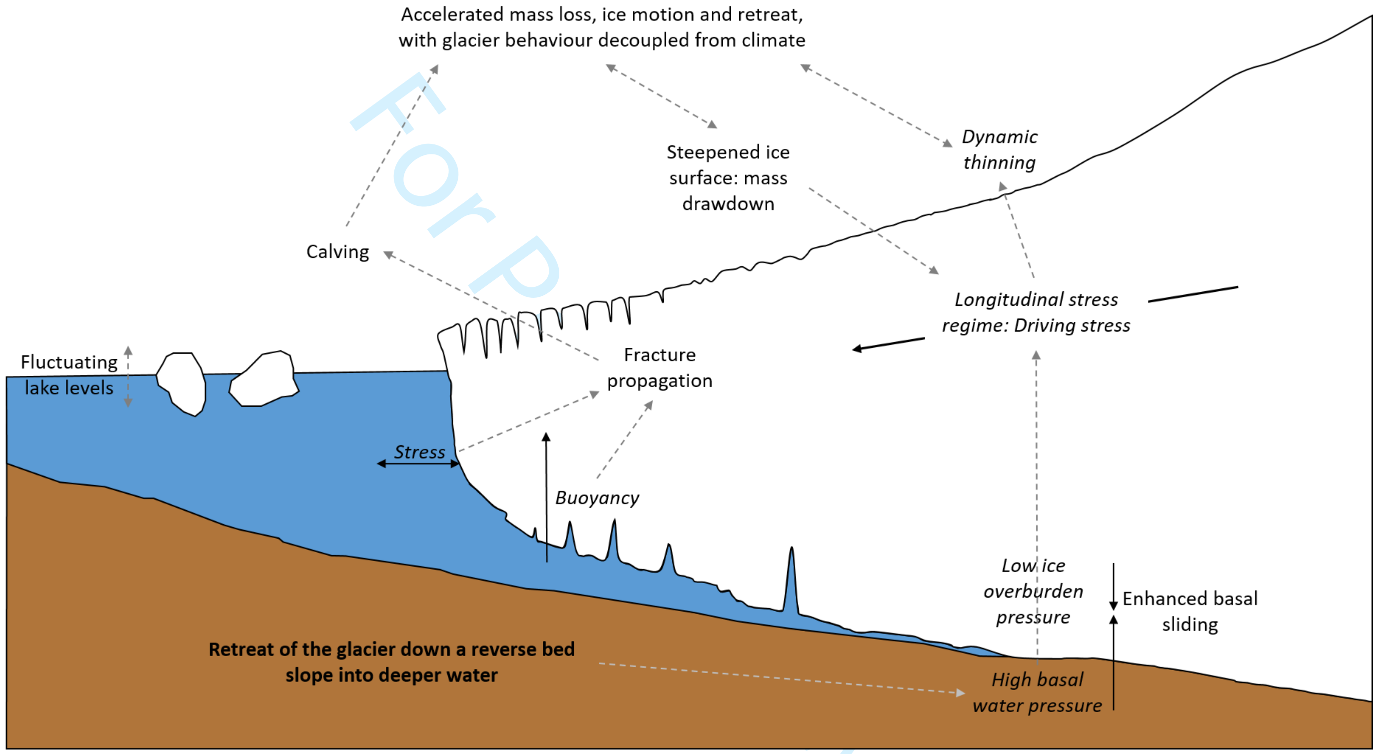

Fig. 11. Summary schematic of the processes occurring at the margin of Fjallsjökull, and the impacts these processes are having on its overall velocity pattern, based on the UAV-SfM data presented in this study. The key forcing mechanism is highlighted in bold and labelled as appropriate. Forces are shown in italicised text with thick black arrows while processes are shown in black text with dashed grey lines to denote interactions. Figure modified from Carrick and Tweed (2013).

The importance of the bedrock channel in forcing the overall behaviour of the glacier is highlighted by the UAV-SfM data, which clearly show that the areas of highest velocities and most negative elevation changes directly coincide with the deepest parts of the bedrock channel. Furthermore, the data from July 2021 also seems to suggest that this dynamic behaviour may have evolved, with higher overall velocities, as well as an increase in the extent of the region characterised by the most negative surface changes, observed during this time in comparison to 2019, reiterating the importance of the bedrock topography in forcing the overall dynamics of Fjallsjökull.

These findings are supported by the results of Dell and others (2019) in their multi-faceted investigation of the evolving dynamics of Fjallsjökull between 1973 and 2017. The authors found that although changes in terminus position and lake area were likely controlled by rising air temperatures since 1973, they also attribute the changing dynamic regime of the glacier to the onset of retreat through its deep basal trough, particularly over recent years. The authors suggest, like is done here, that the trough, and in particular the two deeply incised bedrock channels, have caused an increase in flow acceleration and thinning to occur in these localities, which has led to the implementation of a positive feedback mechanism between retreat, acceleration, surface thinning and calving. The authors also found that the areas of fastest ice flow directly corresponded to the location of these channels, which, they suggest, highlights the key role the subglacial topography has in governing the overall velocity patterns of the glacier (Dell and others, 2019).

However, although the findings of both studies agree that the basal topography of Fjallsjökull has greatly influenced its velocity over recent years, the actual velocities obtained in both studies differ quite substantially. Whereas Dell and others (2019) recorded max velocities of ~0.80 m d^{-1} over the southern bedrock channel; peak values observed in this study from July 2021 are around one and a half times greater, at ~1.2 ±0.11 m d^{-1}. Such discrepancies may be due to the temporal separation between studies, where Dell and others (2019) observed their peak values in 2016/2017, whereas the data here is from 2019 and 2021, and as such, a velocity increase would be expected over this period as the glacier retreats further into its trough. Similarly, as their results are annual velocities, not daily, then it is likely that any seasonal periods of higher velocities may have been averaged out over their longer time period. However, the most plausible reason for the contrast in velocities is the differences in the spatial resolution of the imagery. Dell and others (2019) utilised 10 m resolution Sentinel-2 imagery, whereas the resolution of the UAV-SfM orthomosaics used for the velocity analyses (0.25 m) is ~40 times finer. As a result, fine-scale velocity gradients occurring at the terminus of Fjallsjökull can more easily be picked out and tracked in the UAV-SfM imagery, whereas the coarser resolution of the Sentinel imagery means such gradients will likely have been smoothed-over and missed (Nagler and others, 2015; Rohner and others, 2019). The ability of UAV-SfM imagery to pick out such fine-scale velocity gradients is one of the primary reasons why they have become so popular in glaciological research over recent years, and highlights their importance for investigating the short-term dynamics of fast-flowing calving glaciers, particularly in their near-terminus regions (e.g. Ryan and others, 2015; Jouvet and others, 2019; Rohner and others, 2019).

5.2 Wider Relevance and Implications

5.2.1 Wider Climatological Perspective

One of the most important characteristics of calving glaciers is that their dynamic behaviour can become decoupled from climate, at least partially (Benn and others, 2007; Chernos and others, 2016; Carrivick and others, 2020). This means that other factors which are independent of climate, such as changes in water depth, can often exert a greater influence on the dynamics and retreat patterns of these glaciers (e.g. Meier and Post, 1987; Carrivick and Tweed, 2013; Baurley and others, 2020). These factors are important because they can cause calving glaciers to undergo considerably greater rates of retreat than would otherwise be observed if surface ablation were the sole mass loss mechanism, indicating that these glaciers can often display a highly non-linear response to an initial climatic forcing (Larsen and others, 2007; Sakakibara and others, 2013; Carrivick and others, 2020). Indeed, such a non-linear response can be seen to have occurred at Fjallsjökull over recent decades (Fig. 12).

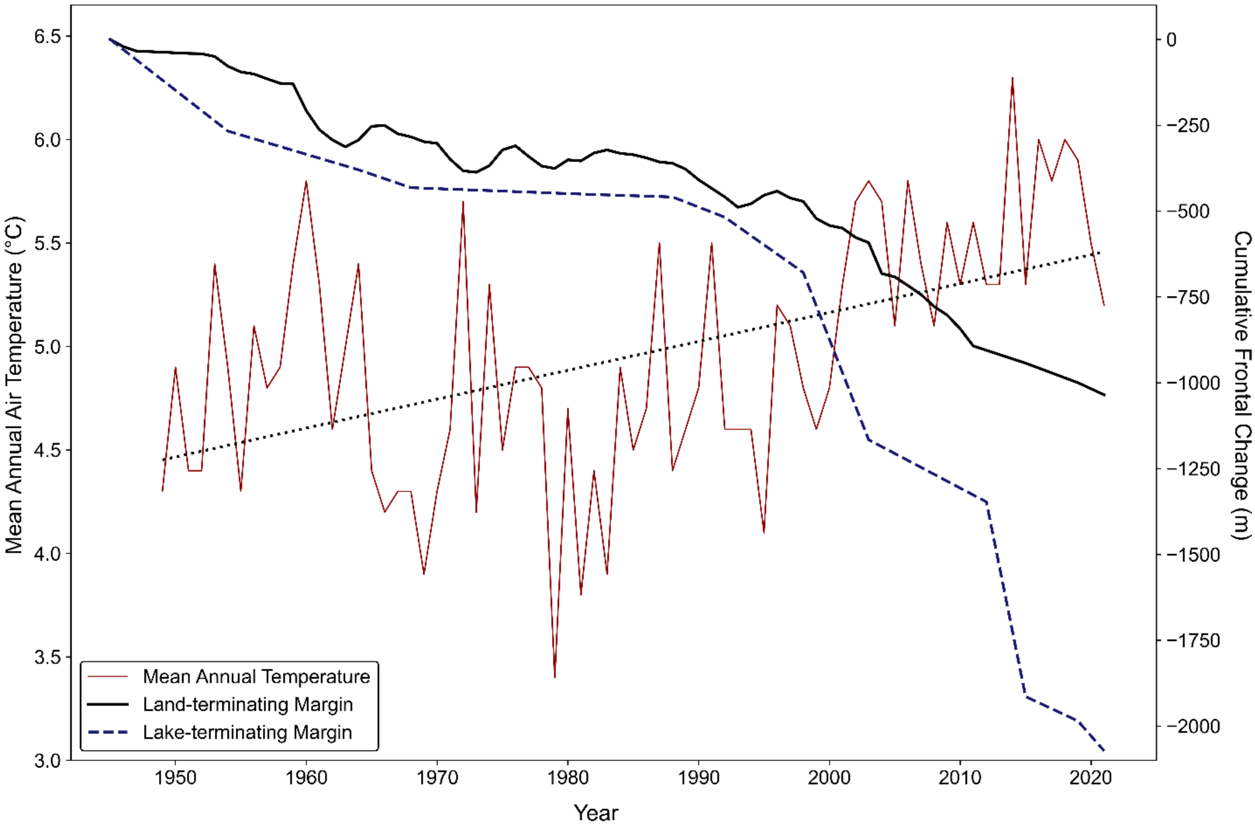

Fig. 12. Mean annual air temperature from the weather station at Fagurhólsmýri (63°53′N, 16°39′W, the nearest long-term weather station to Fjallsjökull, ~20 km to the southwest), plotted alongside the cumulative retreat of Fjallsjökull at its land- and lake-terminating margins for the period 1945-2021. The r^2 for the temperature series is 0.49. Missing data were calculated using a transfer function based on the data recorded by the weather station at Höfn (64°16’N, 15°12’W), which has the second longest meteorological record in Iceland. The retreat data for the land-terminating margin was taken from measurements acquired by the Icelandic Glaciological Society and WGMS, while the data for the lake-terminating margin was calculated using the rectilinear box method, which was applied to selected orthorectified aerial photographs and satellite images from 1945 onwards.

From 1945-1990, the retreat at both the land- and lake-terminating margins demonstrates a similar pattern, which is perhaps unsurprising as for much of the early to mid-20th century the proglacial lake Fjallsárlón was relatively small. This suggests its ability to impact upon the overall velocity or retreat patterns of the glacier was limited (i.e. there was little calving), with this retreat instead being forced by rising air temperatures in the region during this time. However, from 1990 onwards both the land- and lake-terminating margins have retreated at different rates. Indeed, nearly three times as much retreat occurred at the lake-terminating margin than at the land-terminating margin (1554 m compared to 576 m), equating to a retreat rate of -52 m a^{-1} and -19 m a^{-1} respectively, despite both regions undergoing the same climatic forcing (+0.4°C). This clearly indicates that the retreat of the lake-terminating margin during this time has likely been primarily forced by glacier specific factors (i.e. the growth of Fjallsárlón, influence of the bedrock topography and calving processes), rather than by solely rising air temperatures in the region.

This is important as it highlights how the growth of Fjallsárlón, and the dynamic processes that have been initiated as a result, have (at least partially) decoupled Fjallsjökull from the effects of the changing climate. As such, the dynamic response that is now underway is occurring beyond what would be expected through climate alone, i.e. the glacier is losing more mass and retreating more rapidly than would otherwise be observed if it were being forced solely by climate, with such a response predicted to continue until the glacier retreats out of the bedrock trough and into shallower water (Dell and others, 2019). It is worth noting that the role of climate has been, and still is, important for the glacier, both at present and in the future. For example, rates of surface thinning, even over the deepest parts of the trough, will still be influenced to an extent by rising air temperatures, while the retreat of those regions not in contract with the lake will still be forced by surface melt. In addition, once the glacier does retreat out of the trough and into shallower water, its dynamic behaviour and future pattern of retreat will once again be primarily controlled by rising air temperatures (i.e. its behaviour will become coupled to the changing climate). However, the changes that the glacier has undergone over recent years are both too significant, and too rapid to have been forced solely by the observed change in climate. This reiterates the importance of glacier calving, not only for its ability to decouple the behaviour of a glacier from climate, but also for controlling how these glaciers will respond in future, highlighting how further research and continued monitoring of these glaciers is required in order to better predict and understand their future response (Boyce and others, 2007; Sakakibara and others, 2013; Dell and others, 2019; Carrivick and others, 2020).

5.2.2 Basal Topography and its Influence on Ice Dynamics

The heightened dynamic response following retreat into overdeepened basal troughs, as observed here for Fjallsjökull, has also been observed at several other lake-terminating glaciers in Iceland and elsewhere. For example, at Breiðamerkurjökull, the neighbouring glacier to Fjallsjökull, Baurley and others (2020) attributed the recent increase in velocities and retreat of the glacier to the increase in size and depth of its proglacial lake Jökulsárlón, as the glacier retreated into the 200-300 m deep bedrock trough it formed during the LIA. The authors suggest that while initial retreat was instigated by rising air temperatures, once Jökulsárlón increased to a sufficient size where it was able to start influencing frontal retreat and ice flow, then this became the dominant mechanism in causing the rapid retreat, thinning and flow velocities observed since the turn of the 21st century, with such a response likely to continue until the glacier recedes out of the deepest part of the bedrock trough and into shallower water (Baurley and others, 2020).

There is also the strong possibility that the other southern outlets of Vatnajökull will undergo a similar dynamic response in future, as many of these also have reverse-sloping beds that sit some 100-300 m below the current elevation of their termini (Magnússon and others, 2012; Hannesdóttir and others, 2015). Furthermore, these outlets have also seen the development and growth of proglacial lakes at their termini, and although at present these lakes are currently situated in the outermost part of these bedrock troughs, this means they are likely to further grow as these glaciers continue to retreat rapidly in response to warming air temperatures (Hannesdóttir and others, 2015; Guðmundsson and others, 2019). Consequently, these glaciers will likely recede down their reverse-sloping beds into deeper water, increasing velocities, calving, and initiating a dynamic response similar to that observed here for Fjallsjökull and by Baurley and others (2020) for Breiðamerkurjökull, leading to a pattern of rapid retreat and mass loss that is (at least partially) decoupled from climate (Guðmundsson and others, 2019).

Elsewhere, at Mendenhall Glacier, Alaska, Motyka and others (2003) found that as the glacier thinned and retreated into deeper water, the buoyant forces acting on the terminus increased, allowing the terminus to reach floatation and begin to destabilise. Once underway, the terminus began to calve at an increased rate, causing the glacier to retreat further into deeper water and initiating a positive feedback mechanism (Motyka and others, 2003). Similar patterns of mass loss were also found for several other large lake-terminating glaciers in Alaska by Larsen and others (2007). Meanwhile, Sakakibara and others (2013) attributed the observed recession and acceleration since 2008 at Glacier Upsala, Patagonia, to a change in the longitudinal stress exerted by the bed in response to the glacier retreating over a bedrock rise and down a reverse slope into deeper water.

Similarly, Liu and others (2020) in their multi-decadal study of the dynamics of Longbasaba Glacier, Chinese Himalaya from 1989-2018 attributed the observed onset of fast velocities and rapid frontal retreat to the detachment of the glacier from its terminal moraine and recession down a reverse-bed slope into its ~100 m deep basal trough. The authors argued that such high rates of frontal retreat must be balanced by drawdown of ice from further up-glacier, leading to dynamic thinning over a large area of the glacier, which they observed to be occurring in the latter years of their study (Liu and others, 2020). Similar dynamic responses of lake-terminating Himalayan glaciers to changes in water depth have also been observed by King and others (2018) and Tsutaki and others (2019) for the Central and Bhutanese Himalaya, respectively.

Although there are notable differences between the processes influencing lake-terminating glaciers in Iceland compared to those glaciers elsewhere, there are many clear similarities in their overall dynamics. In particular, the feedback mechanism that can be introduced once a glacier starts retreating down a reverse-bed slope into deeper water is extremely important, particularly because it can lead to very high rates of mass loss and frontal retreat above what may be predicted based on current observations (Carrivick and Tweed, 2013; Baurley and others, 2020). There is a need, therefore, to investigate these processes further and to monitor these glaciers more closely so that their likely future response can be more accurately predicted under a changing climate (Carrivick and others, 2020; Shugar and others, 2020).

6. CONCLUSION

We have investigated the changing dynamic behaviour of Fjallsjökull, a large lake-terminating glacier in southeast Iceland, over the 2019 and 2021 ablation season using repeat high-resolution UAV-SfM methods. Our data demonstrate that both the highest velocities, and most negative elevation changes are consistently found towards the northern part of the study region, corresponding to the location of a 100-120 m deep bedrock channel. Velocities in this region peak at ~0.95 m d^{-1} in 2019, increasing up to 1.2 m d^{-1} in 2021, whilst up to 2.50 ±0.18 m, and ~5.50 ±0.15 m of negative surface changes are also observed here in 2019 and 2021, respectively.

We suggest these elevated velocities are strongly controlled by the ongoing retreat of the glacier through the deepest part of the deep bedrock channel, which has caused an increase in water depth at the terminus. This has triggered an increase in ice velocity, causing the glacier surface to undergo longitudinal stretching, permitting crevasse propagation, and thus calving. This has resulted in increased mass loss and frontal retreat, leading to a further increase in velocities, longitudinal stretching, and the implementation of the dynamic thinning feedback mechanism. Our data also seem to indicate that this dynamic behaviour may have evolved through time, with higher overall velocities, and an increase in the extent of the region characterised by the most negative surface changes, observed in July 2021 compared to July 2019. As such, these processes, forced primarily by the retreat of Fjallsjökull into deeper water, suggest the underlying bedrock topography is exerting a first order control on the overall dynamics of the glacier.

Our data also indicate that the overall dynamic behaviour of the glacier has become decoupled from the changing climate, at least partially. Indeed, such a dynamic response is occurring beyond what would be expected through climate alone, with this predicted to continue in future until the glacier retreats out of the deepest parts of the bedrock channel into shallower water. Such a dynamic response may also be analogous for those processes that have already occurred, or may occur in future, at other lake-terminating glaciers in southeast Iceland, which are also beginning to retreat into their own deep bedrock troughs. In addition, similar dynamic behaviour, linked to the presence of deep bedrock troughs, has also been observed at several lake-terminating glaciers in other glaciated regions, and as such our findings may provide an indication as to how similar lake-terminating glaciers in other glaciated regions may also respond in future.

CONFLICT OF INTEREST STATEMENT

The authors declare that the research was conducted in the absence of any commercial or financial relationships that could be construed as a potential conflict of interest.

DATA AVAILABILITY STATEMENT

The datasets generated for this study can be found in the following repositories: https://doi.org/10.5281/zenodo.7105133 and https://doi.org/10.5281/zenodo.7111111.

AUTHOR CONTRIBUTIONS

NB and JH devised the study. NB undertook the fieldwork, processed and analysed the UAV data and wrote the draft version of the manuscript. Both authors contributed to the writing and editing of the final manuscript.

ACKNOWLEGEMENTS

NB wishes to thank David Sutherland and Chris Tomsett for their assistance across the three field campaigns, as well as the Vatnajökull National Park for providing a research permit to allow each of the three campaigns to be undertaken. The authors also thank Eyjólfur Magnússon for sharing his bedrock topography data for Fjallsjökull. NB acknowledges funding from several sources: The first field campaign in July 2019 was funded by a Postgraduate Research Award from the Royal Geographical Society (with IBG), the second in September 2019 by a NRWA from the Quaternary Research Association and an expedition grant from The Mount Everest Foundation, and the third in July 2021 by a Dudley Stamp Memorial Award (part of the Postgraduate Research Awards) from the Royal Geographical Society (with IBG), and an expedition grant from The Mount Everest Foundation.

REFERENCES

Agisoft LLC (2021) Agisoft Metashape User Manual: Professional edition, Version 1.7. [online]. Agisoft LLC. Available from: https://www.agisoft.com/downloads/user-manuals/ [Accessed: 23rd September 2021].

Altena B and Kääb A (2017) Glacier ice loss monitored through the Planet cubesat constellation. In *2017 9th International Workshop on the Analysis of Multitemporal Remote Sensing Images (MultiTemp)* (1-4), Brugge, Belgium. *IEEE*. (doi: 10.1109/Multi-Temp.2017.8035235)

Bash EA, Moorman BJ and Gunther A (2018) Detecting short-term surface melt on an Arctic Glacier using UAV surveys. *Remote Sens.*, **10**(10), 1-17. (doi: 10.3390/rs10101547)

Baurley NR, Robson BA and Hart JK (2020) Long-term impact of the proglacial lake Jökulsárlón on the flow velocity and stability of Breiðamerkurjökull glacier, Iceland. *Earth Surf. Process. Landf.*, **45**(11), 2647-2663. (doi: 10.1002/esp.4920)

Baurley NR, Tomsett C and Hart JK (2022) Assessing UAV-based laser scanning for monitoring glacial processes and interactions at high spatial and temporal resolutions. *Front. Remote Sens.*, **3**, 1027065. (doi: 10.3389/frsen.2022.1027065

Benn DI, Warren CR and Mottram RH (2007) Calving processes and the dynamics of calving glaciers. *Earth-Sci. Rev.*, **82**(3-4), 143-179. (doi: 10.1016/j.earscirev.2007.02.002)

Benn DI and Åström JA (2018) Calving glaciers and ice shelves. *Adv. Phys-X*, **3**(1), 1513819. (doi: 10.1080/23746149.2018.1513819)

Boyce ES, Motyka RJ and Truffer M (2007) Flotation and retreat of a lake-calving terminus, Mendenhall Glacier, southeast Alaska, USA. *J. Glaciol.*, **53**(181), 211-224. (doi: 10.3189/172756507782202928)

Carrivick JL and Tweed FS (2013) Proglacial lakes: Character, behaviour and geological importance. *Quat. Sci. Rev.*, **78**, 34-52. (doi: 10.1016/j.quascirev.2013.07.028)

Carrivick JL, Tweed FS, Sutherland JL and Mallalieu J (2020) Toward numerical modelling of interactions between ice-marginal proglacial lakes and glaciers. *Front. Earth Sci.*, **8**, 577068. (doi: 10.3389/feart.2020.577068)

Chandler, BM and 7 others (2020) The glacial landsystem of Fjallsjökull, Iceland: Spatial and temporal evolution of process-form regimes at an active temperate glacier. *Geomorphology*, **361**(107192), 1-28. (doi: 10.1016/j.geomorph.2020.107192)

Chernos M, Koppes M and Moore RD (2016) Ablation from calving and surface melt at lake-terminating Bridge Glacier, British Columbia, 1984-2013. *Cryosphere*, **10**(1), 87-102. (doi: 10.5194/tc-10-87-2016)

Chudley T, Christoffersen P, Doyle SH, Abellan A and Snooke N (2019) High accuracy UAV photogrammetry of ice sheet dynamics with no ground control. *Cryosphere*, **13**(3), 955-968. (doi: 10.5194/tc-13-955-2019)

Chudley, TR and 7 others (2021) Controls on water storage and drainage in crevasses on the Greenland Ice Sheet. *J. Geophys. Res. Earth Surf.*, **126**(9), 2021JF006287. (doi 10.1029/2021JF006287)

Dehecq A, Gourmelen N and Trouvé E (2015) Deriving large-scale glacier velocities from a complete satellite archive: Application to the Pamir-Karakoram-Himalaya. *Remote Sens. Environ.*, **162**, 55-66. (doi: 10.1016/j.rse.2015.01.031)

Dell R, Carr R, Phillips E and Russell AJ (2019) Response of glacier flow and structure to proglacial lake development and climate at Fjallsjökull, south-east Iceland. *J. Glaciol.*, **65**(250), 321-336. (doi: 10.1017/jog.2019.18)

DJI (2021) Zenmuse X4S Specs. [online]. https://www.dji.com/uk/zenmuse-x4s/info#specs. [Accessed: 16th September 2021].

Ely JC, Graham C, Barr ID, Rea BR, Spagnolo M and Evans J (2017) Using UAV acquired photography and structure from motion techniques for studying glacier landforms: Application to the glacial flutes at Isfallsglaciären. *Earth Surf. Process. Landf.*, **42**(6), 877-888. (doi: 10.1002/esp.4044)

Emlid (2021a) Emlid Reach. [online]. Available at: https://emlid.com/reach/. [Accessed 16th September 2021].

Emlid (2021b) Understanding PPK solution and analyzing logs from Reach. [online]. Available at: https://docs.emlid.com/reach/tutorials/post-processing-workflow/analyzing-logs. [Accessed: 23rd September 2021].

Evans DJ and Twigg DR (2002) The active temperate glacial landsystem: A model based on Breiðamerkurjökull and Fjallsjökull, Iceland. *Quat. Sci. Rev.*, **21**(20-22), 2143-2177. (doi: 10.1016/S0277-3791(02)00019-7)

Farinotti, D and 6 others (2019) A consensus estimate for the ice thickness distribution of all glaciers on Earth. *Nat. Geosci.*, **12**(3), 168-173. (doi: 10.1038/s41561-019-0300-3)

Fonstad MA, Dietrich JT, Courville BC, Jensen JL and Carbonneau PE (2013) Topographic structure from motion: A new development in photogrammetric measurement. *Earth Surf. Process. Landf.*, **38**(4), 421-430. (doi: 10.1002/esp.3366)

Gardner, AS and 15 others (2013) A reconciled estimate of glacier contributions to sea level rise: 2003 to 2009. *Science*, **340**(6134), 852-857. (doi: 10.1126/science.1234532)

Gärtner-Roer I, Nussbaumer SU, Hüsler F and Zemp M (2019) Worldwide assessment of national glacier monitoring and future perspectives. *Mt. Res. Dev.*, **39**(2), A1-A11. (doi: 10.1659/MRD-JOURNAL-D-19-00021.1)

Gindraux S, Boesch R and Farinotti D (2017) Accuracy assessment of digital surface models from unmanned aerial vehicles' imagery on glaciers. *Remote Sens.*, **9**(2), 1-15. (doi: 10.3390/rs9020186)

Guðmundsson S, Björnsson H, Pálsson F, Magnússon E, Sæmundsson Þ and Jóhannesson T (2019) Terminus lakes on the south side of Vatnajökull ice cap, SE-Iceland. *Jökull*, **69**, 1-34.

Hannesdóttir H, Björnsson H, Pálsson F, Aðalgeirsdóttir G and Guðmundsson S (2015) Changes in the southeast Vatnajökull ice cap, Iceland, between ~1890 and 2010. *Cryosphere*, **9**(2), 565-585. (doi: 10.5194/tc-9-565-2015)

Haug T, Kääb A and Skvarca P (2010) Monitoring ice shelf velocities from repeat MODIS and Landsat data-a method study on the Larsen C ice shelf, Antarctic Peninsula, and 10 other ice shelves around Antarctica. *Cryosphere*, **4**(2), 161-178. (doi: 10.5194/tc-4-161-2010)

Heid T and Kääb A (2012) Evaluation of existing image matching methods for deriving glacier surface displacements globally from optical satellite imagery. *Remote Sens. Environ.*, **118**, 339-355. (doi: 10.1016/j.rse.2011.11.024)

Herman F, Anderson B and Leprince S (2011) Mountain glacier velocity variation during a retreat/advance cycle quantified using sub-pixel analysis of ASTER images. *J. Glaciol.*, **57**(202), 197-207. (doi: 10.3189/002214311796405942)

Höhle J and Höhle M (2009) Accuracy assessment of digital elevation models by means of robust statistical methods. *ISPRS J. Photogramm. Remote Sens.*, **64**(4), 398-406. (doi: 10.1016/j.isprsjprs.2009.02.003)

How, P and 8 others (2019) Calving controlled by melt-under-cutting: Detailed calving styles revealed through time-lapse observations. *Ann. Glaciol.*, **60**(78), 20-31. (doi: 10.1017/aog.2018.28)

Howat IM, Joughin I and Scambos TA (2007) Rapid changes in ice discharge from Greenland outlet glaciers. *Science*, **315**(5818), 1559-1561. (doi: 10.1126/science.1138478)

Howat IM, Joughin I, Fahnestock M, Smith BE and Scambos TA (2008) Synchronous retreat and acceleration of southeast Greenland outlet glaciers 2000–06: Ice dynamics and coupling to climate. *J. Glaciol.*, **54**(187), 646-660. (doi: 10.3189/002214308786570908)

Hugonnet, R and 10 others (2021) Accelerated global glacier mass loss in the early twenty-first century. *Nature*, **592**(7856), 726-731. (doi: 10.1038/s41586-021-03436-z)

Huss M and Hock R (2015) A new model for global glacier change and sea-level rise. *Front. Earth Sci.*, **3**, 54. (doi: 10.3389/feart.2015.00054)

Huss M and Hock R (2018) Global-scale hydrological response to future glacier mass loss. *Nat. Clim. Chang.*, **8**(2), 135-140. (doi: 10.1038/s41558-017-0049-x)

Immerzeel, WW and 6 others (2014) High-resolution monitoring of Himalayan glacier dynamics using unmanned aerial vehicles. *Remote Sens. Environ.*, **150**, 93-103. (doi: 10.1016/j.rse.2014.04.025)

James MR and Robson S (2012) Straightforward reconstruction of 3D surfaces and topography with a camera: Accuracy and geoscience application. *J. Geophys. Res. Earth Surf.*, **117**(F3). (doi: 10.1029/2011JF002289)

Jouvet G, Weidmann Y, van Dongen E, Luethi M, Vieli A and Ryan J (2019) High-endurance UAV for monitoring calving glaciers: Application to the Inglefield Bredning and Eqip Sermia, Greenland. *Front. Earth Sci.*, **7**, 206. (doi: 10.3389/feart.2019.00206)

Kim Y and Bang H (2019) Introduction to Kalman filter and its applications, in Govaers, F (ed.) *Introduction and Implementations of the Kalman Filter*. London: IntechOpen, 7-22. (doi: 10.5772/intechopen.80600)

King O, Dehecq A, Quincey D and Carrivick J (2018) Contrasting geometric and dynamic evolution of lake and land-terminating glaciers in the central Himalaya. *Glob. Planet. Change*, **167**, 46-60. (doi: 10.1016/j.gloplacha.2018.05.006)

Kraaijenbrink P, Meijer SW, Shea JM, Pellicciotti F, De Jong SM and Immerzeel WW (2016) Seasonal surface velocities of a Himalayan glacier derived by automated correlation of unmanned aerial vehicle imagery. *Ann. Glaciol.*, **57**(71), 103-113. (doi: 10.3189/2016AoG71A072)

Larsen CF, Motyka RJ, Arendt AA, Echelmeyer KA and Geissler PE (2007) Glacier changes in southeast Alaska and northwest British Columbia and contribution to sea level rise. *J. Geophys. Res. Earth Surf.*, **112**(F1). (doi: 10.1029/2006JF000586)

Lague D, Brodu N and Leroux J (2013) Accurate 3D comparison of complex topography with terrestrial laser scanner: Application to the Rangitikei canyon (NZ). *ISPRS J. Photogramm. Remote Sens.*, **82**, 10-26. (doi: 10.1016/j.isprsjprs.2013.04.009)

Lemos A, Shepherd A, McMillan M and Hogg AE (2018) Seasonal variations in the flow of land-terminating glaciers in Central-West Greenland using Sentinel-1 imagery. *Remote Sens.*, **10**(12), 1878. (doi: 10.3390/rs10121878)

Liu, Q and 6 others (2020) Interannual flow dynamics driven by frontal retreat of a lake-terminating glacier in the Chinese Central Himalaya. *Earth Planet. Sci. Lett.*, **546**, 116450. (doi: 10.1016/j.epsl.2020.116450)

Magnússon E, Pálsson F, Björnsson H and Guðmundsson S (2012) Removing the ice cap of Öræfajökull central volcano, SE Iceland: Mapping and interpretation of bedrock topography, ice volumes, subglacial troughs and implications for hazards assessments. *Jökull*, **62**, 131-150.

Marzeion, B and 16 others (2020) Partitioning the uncertainty of ensemble projections of global glacier mass change. *Earth's Future*, **8**(7), e2019EF001470. (doi: 10.1029/2019EF001470)

Meier MF and Post A (1987) Fast tidewater glaciers. *J. Geophys. Res. Solid Earth*, **92**(B9), 9051-9058. (doi: 10.1029/JB092iB09p09051)

Millan, R and 6 others (2019) Mapping surface flow velocity of glaciers at regional scale using a multiple sensors approach. *Remote Sens.*, **11**(21), 2498. (doi: 10.3390/rs11212498)

Motyka RJ, O'Neel S, Connor CL and Echelmeyer KA (2003) Twentieth century thinning of Mendenhall Glacier, Alaska, and its relationship to climate, lake calving, and glacier run-off. *Glob. Planet. Change*, **35**(1-2), 93-112. (doi: 10.1016/S0921-8181(02)00138-8)

Nagler T, Rott H, Hetzenecker M, Wuite J and Potin P (2015) The Sentinel-1 mission: New opportunities for ice sheet observations. *Remote Sens.*, **7**(7), 9371-9389. (doi: 10.3390/rs70709371)

Paul, F and 10 others (2015) The glaciers climate change initiative: Methods for creating glacier area, elevation change and velocity products. *Remote Sens. Environ.*, **162**, 408-426. (doi: 10.1016/j.rse.2013.07.043)

Pronk JB, Bolch T, King O, Wouters B and Benn DI (2021) Contrasting surface velocities between lake-and land-terminating glaciers in the Himalayan region. *Cryosphere*, **15**(12), 5577-5599. (doi: 10.5194/tc-15-5577-2021)

Purdie HL, Brook MS and Fuller IC (2008) Seasonal variation in ablation and surface velocity on a temperate maritime glacier: Fox Glacier, New Zealand. *Arct. Antarc. Alp. Res.*, **40**(1), 140-147. (doi: 10.1657/1523-0430(06-032)[PURDIE]2.0.CO;2)

Robson BA, Nuth C, Nielsen PR, Girod, L, Hendrickx M and Dahl SO (2018) Spatial variability in patterns of glacier change across the Manaslu Range, Central Himalaya. *Front. Earth Sci.*, **6**, 12. (doi: 10.3389/feart.2018.00012)

Rohner C, Small D, Beutel J, Henke D, Lüthi MP and Vieli A (2019) Multisensor validation of tidewater glacier flow fields derived from synthetic aperture radar (SAR) intensity tracking. *Cryosphere*, **13**(11), 2953-2975. (doi: 10.5194/tc-13-2953-2019)

Rossini, M and 7 others (2018) Rapid melting dynamics of an alpine glacier with repeated UAV photogrammetry. *Geomorphology*, **304**, 159-172. (doi: 10.1016/j.geomorph.2017.12.039)

Ryan, JC and 7 others (2015) UAV photogrammetry and structure from motion to assess calving dynamics at Store Glacier, a large outlet draining the Greenland ice sheet. *Cryosphere*, **9**, 1-11. (doi: 10.5194/tc-9-1-2015)

Sakakibara D, Sugiyama S, Sawagaki T, Marinsek S and Skvarca P (2013) Rapid retreat, acceleration and thinning of Glaciar Upsala, Southern Patagonia Icefield, initiated in 2008. *Ann. Glaciol.*, **54**(63), 131-138. (doi: 10.3189/2013AoG63A236)

Sakakibara D and Sugiyama S (2014) Ice-front variations and speed changes of calving glaciers in the Southern Patagonia Icefield from 1984 to 2011. *J. Geophys. Res. Earth Surf.*, **119**(11), 2541-2554. (doi: 10.1002/2014JF003148)

Sakakibara D and Sugiyama S (2018) Ice front and flow speed variations of marine-terminating outlet glaciers along the coast of Prudhoe Land, northwestern Greenland. *J. Glaciol.*, **64**(244), 300-310. (doi: 10.1017/jog.2018.20)

Shapero DR, Joughin IR, Poinar K, Morlighem M and Gillet-Chaulet F (2016) Basal resistance for three of the largest Greenland outlet glaciers. *J. Geophys. Res. Earth Surf.*, **121**(1), 168-180. (doi: 10.1002/2015JF003643)

Shugar, DH and 9 others (2020) Rapid worldwide growth of glacial lakes since 1990. *Nat. Clim. Chang.*, **10**(10), 939-945. (doi: 10.1038/s41558-020-0855-4)

Snavely, KN (2008) *Scene reconstruction and visualization from internet photo collections* (PhD thesis, University of Washington).

Storrar RD, Jones AH and Evans DJ (2017) Small-scale topographically-controlled glacier flow switching in an expanding proglacial lake at Breiðamerkurjökull, SE Iceland. *J. Glaciol.*, **63**(240), 745-750. (doi: 10.1017/jog.2017.22)

Sugiyama, S and 7 others (2011) Ice speed of a calving glacier modulated by small fluctuations in basal water pressure. *Nat. Geosci.*, **4**(9), 597-600. (doi: 10.1038/ngeo1218)

Sugiyama S, Sakakibara D, Tsutaki S, Maruyama M and Sawagaki T (2015) Glacier dynamics near the calving front of Bowdoin Glacier, northwestern Greenland. *J. Glaciol.*, **61**(226), 223-232. (doi: 10.3189/2015JoG14J127)

Tomsett C and Leyland J (2021) Development and Testing of a UAV Laser Scanner and Multispectral Camera System for Eco-Geomorphic Applications. *Sensors*, **21**(22), 7719. (doi: 10.3390/s21227719)

Truffer M and Motyka RJ (2016) Where glaciers meet water: Subaqueous melt and its relevance to glaciers in various settings. *Rev. Geophys.*, **54**(1), 220-239. (doi: 10.1002/2015RG000494)

Trüssel BL, Motyka RJ, Truffer M and Larsen CF (2013) Rapid thinning of lake-calving Yakutat Glacier and the collapse of the Yakutat Icefield, southeast Alaska, USA. *J. Glaciol.*, **59**(213), 149-161. (doi: 10.3189/2013J0G12J081)

Tsutaki S, Sugiyama S, Nishimura D and Funk M (2013) Acceleration and flotation of a glacier terminus during formation of a proglacial lake in Rhonegletscher, Switzerland. *J. Glaciol.*, **59**(215), 559-570. (doi: 10.3189/2013JoG12J107)

Tsutaki, S and 6 others (2019) Contrasting thinning patterns between lake-and land-terminating glaciers in the Bhutanese Himalaya. *Cryosphere*, **13**(10), 2733-2750. (doi: 10.5194/tc-13-2733-2019)

Warren CR and Kirkbride MP (2003) Calving speed and climatic sensitivity of New Zealand lake-calving glaciers. *Ann. Glaciol.*, **36**, 173-178. (doi: 10.3189/172756403781816446)

Westoby MJ, Brasington J, Glasser NF, Hambrey MJ and Reynolds JM (2012) 'Structure-from-Motion' photogrammetry: A low-cost, effective tool for geoscience applications. *Geomorphology*, **179**, 300-314. (doi: 10.1016/j.geomorph.2012.08.021)

WGMS (2020) Fluctuations of Glaciers Database. World Glacier Monitoring Service, Zurich, Switzerland. (doi: 10.5904/wgms-fog-2020-08)

Whitehead K, Moorman BJ and Hugenholtz CH (2013) Brief Communication: Low-cost, on-demand aerial photogrammetry for glaciological measurement. *Cryosphere*, **7**(6), 1879-1884. (doi: 10.5194/tc-7-1879-2013)

Wigmore O and Mark BG (2017) Monitoring tropical debris-covered glacier dynamics from high-resolution unmanned aerial vehicle photogrammetry, Cordillera Blanca, Peru. *Cryosphere*, **11**, 2463-2480. (doi: 10.5194/tc-11-2463-2017)

Wouters B, Gardner AS and Moholdt G (2019) Global glacier mass loss during the GRACE satellite mission (2002-2016). *Front. Earth Sci.*, **7**, 96. (doi: 10.3389/feart.2019.00096)

Xue Y, Jing Z, Kang S, He X and Li C (2021) Combining UAV and Landsat data to assess glacier changes on the central Tibetan Plateau. *J. Glaciol.*, **67**(265), 1-13. (doi: 10.1017/jog.2021.37)

Yang, W and 8 others (2020) Seasonal Dynamics of a Temperate Tibetan Glacier Revealed by High-Resolution UAV Photogrammetry and In Situ Measurements. *Remote Sens.*, **12**(15), 2389. (doi: 10.3390/rs12152389)

Zemp, M and 14 others (2019) Global glacier mass changes and their contributions to sea-level rise from 1961 to 2016. *Nature*, **568**(7752), 382-386. (doi: 10.1038/s41586-019-1071-0)